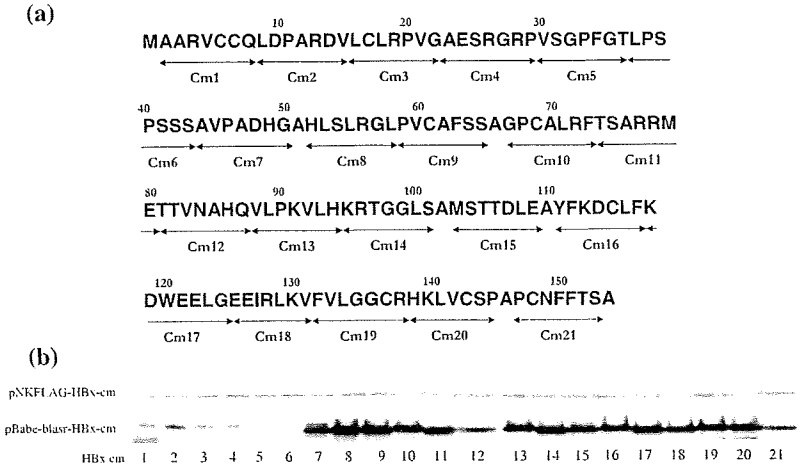

Fig. 5. Expression of hepatitis B virus X protein (HBx) library of clustered alanine substitution mutants in BJ-human telomerase reverse transcriptase (hTERT) cells. (a) Schematic representations of a series of clustered alanine substitution mutants (cm1 to cm21) of HBx. The amino acid locations of the clustered mutations are shown. (b) Detection of the mutated HBx proteins. Total cell lysates prepared from BJ-hTERT cells transfected with the mutant HBx expression vectors were fractionated by sodium dodecylsulfate–polyacrylamide gel electrophoresis and subjected to western blot analysis with anti-FLAG M2 antibody.

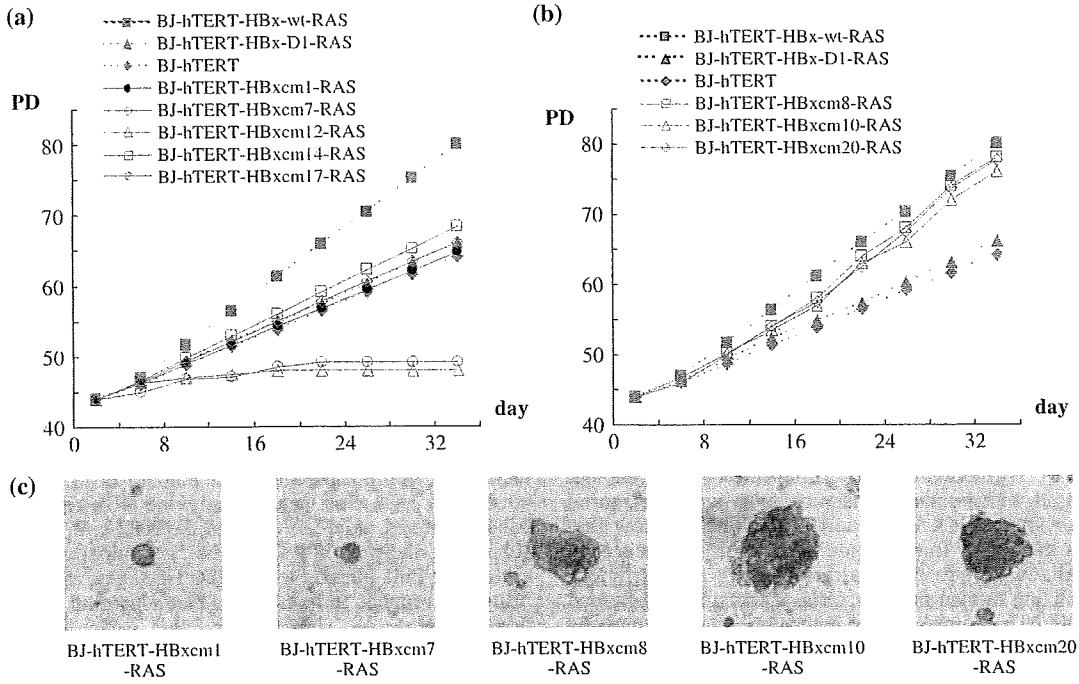

Fig. 6. Critical regions of hepatitis B virus X protein (HBx)-wt for tumorigenic function. (a) Effect of HBx-cm1–7 and HBx-cm11–18 failed to overcome H-RAS^{V12}-induced cellular senescence. Cell proliferation curves of several HBx-cm clones introduced with BJ-human telomerase reverse transcriptase (hTERT)-H-RAS$^{V(12)}$ in addition to those of BJ-hTERT cells (filled diamonds), H-RAS^{V12}-introduced BJ-hTERT-HBx-wt cells (filled squares) and BJ-hTERT-HBx-D1 cells (filled triangles) are shown. HBx-cm1, -cm7, -cm12, -cm14 and -cm17 were selected. HBx-cm1 (closed circles) and HBx-cm7 (open diamonds) represent HBx-cm1–7-introduced BJ-hTERT-H-RAS^{V12} cells. HBx-cm12 (open triangles) represents HBx-cm11–13-introduced BJ-hTERT-H-RAS^{V12} cells. HBx-cm14 (open squares) represents HBx-cm14–16-introduced BJ-hTERT-H-RAS^{V12} cells. HBx-cm17 (open circles) represents HBx-cm17 and HBx-cm18-introduced BJ-hTERT-H-RAS^{V12} cells. pBabe-puro-RAS-infected cells were selected with 1 μg/mL puromycin. After 10 days of drug selection at population doubling (PD) 44, triplicate samples of 1×10^5 cells were plated and grown under normal conditions. (b) Effect of HBx-cm8–10 and HBx-cm19–21 overcomes H-RAS^{V12}-induced cellular senescence. Cell proliferation curves of several HBx-cm clones introduced into BJ-hTERT-H-RAS^{V12} in addition to those of BJ-hTERT cells (filled diamonds), H-RAS^{V12}-introduced BJ-hTERT-HBx-wt cells (filled square) and BJ-hTERT-HBx-D1 cells (filled triangles) are shown. HBx-cm8 (open squares) and HBx-cm10 (open triangles) represent HBx-cm8–10-introduced BJ-hTERT-H-RAS^{V12} cells. HBx-cm20 (open diamonds) represents HBx-cm19–21-introduced BJ-hTERT-H-RAS^{V12} cells.

and HBx-cm18 were found to be critical for overcoming active RAS-induced senescence as the BJ-hTERT-RAS clones expressing these HBx-cm mutants failed to proliferate, meaning that these had no ability to overcome active RAS-induced cellular senescence at all (Fig. 6) (Table 1). Among the BJ-hTERT-HBx-cm cells, expression levels of HBx-cm1 to HBx-cm6 were very weak, like that of HBx-D1. Furthermore, the protein bands of HBx-cm1 to HBx-cm5 migrated slightly slower than those of HBx-cm6 and the other HBx-cm mutants in the coactivation domain in SDS-PAGE analysis (see Discussion).

doi: 10.1111/j.1349-7006.2007.00579.x

Table 1. Degree of proliferation of H-RAS^{V12}-introduced BJ-hTERT-HBx-cm cells

Cell type	Degree of proliferation
HBx-cm1†	+‡
HBx-cm2	+
HBx-cm3	+
HBx-cm4	+
HBx-cm5	+
HBx-cm6	+
HBx-cm7	+
HBx-cm8	++§
HBx-cm9	++
HBx-cm10	++
HBx-cm11	–
HBx-cm12	–¶
HBx-cm13	–
HBx-cm14	+
HBx-cm15	+
HBx-cm16	+
HBx-cm17	–
HBx-cm18	–
HBx-cm19	++
HBx-cm20	++
HBx-cm21	++

†HBx-cm1–21 in this table represent HBx-cm1–21-introduced BJ-hTERT-H-RAS^{V12} cells. ‡Same as BJ-hTERT-HBx-D1-H-RAS^{V12} cells. §Same as BJ-hTERT-HBx-wt-H-RAS^{V12} cells. ¶Senescence.

Discussion

Hepatitis B virus X protein has long been suspected to be positively involved in HBV-associated HCC, but its molecular role in hepatocarcinogenesis remains unclear. Although HBx is involved directly in the transformation of immortal rodent cells *in vitro* and in tumor formation in the livers of nude mice, the oncogenic activity of HBx itself remains to be elicited as the reproducibility of these experiments has been seriously controversial.[5] Furthermore, the positive role of HBx has not been addressed with human primary cells or human immortal cells. To our knowledge, our report is the first to show that HBx retains the ability to overcome RAS-induced senescence of immortalized human cells, although it is not sufficient for immortalizing human primary cells or transforming human immortal cells. hTERT-immortalized human cells stably expressing HBx-wt and RAS can form colonies in soft agar and tumors in nude mice in a cell-number-dependent manner. HBx can overcome RAS-induced senescence of BJ cells, but HBx-wt and active RAS could not immortalize the human fibroblasts. Although our findings are different to a report showing that HBx itself retains the transforming ability in NIH3T3 cells,[9] they are similar to results in rodent immortal embryonic fibroblast cells.[10]

To determine the region of HBx responsible for the ability to overcome RAS-induced senescence, we used two truncation mutants: HBx-D1 (aa 51–154), which exhibits transcriptional coactivation function and augments HBV transcription and replication,[8] and HBx-D5 (aa 1–50), which harbors the negative regulatory domain of transcriptional modulation.[6] When HBx-D1 and H-RAS^{V12} were introduced into BJ-hTERT cells, HBx-D1 was similar to wild-type HBx in overcoming RAS-induced senescence in the PD analysis and in SA-β-gal staining. Therefore, HBx-D1 alone seems to be sufficient for overcoming active RAS-induced senescence and for anchorage-independent growth, but it is not sufficient for BJ-hTERT + H-RAS^{V12} + HBx-D1 cells to form visible colonies in soft agar and tumors in nude mice. HBx alone may be sufficient for overcoming RAS-induced senescence, but hTERT is required for immortal proliferation of the transformed cells with H-RAS^{V12} and HBx. As HBx-D1 exhibits a similar ability to HBx-wt in overcoming RAS-induced senescence and anchorage-independent growth, but not in immortalizing human fibroblasts, HBx-D1 may harbor all of the critical abilities of HBx. However, HBx-D1 is different from HBx-wt in the ability to form visible colonies in soft agar and to form tumors in nude mice.

The coactivation function was recently mapped by scanning a HBx library of clustered alanine substitution mutants (HBx-cm library), and two separate sequences in HBx-D1 were found to be critical.[8] Using the same HBx-cm library, we attempted to map the sequences critical for overcoming RAS-induced senescence. We have identified three different phenotypes among the HBx-cm mutants: those phenotypes are like HBx-wt, HBx-D1 and HBx-D5 (Fig. 6). HBx-cm mutations within the D5 region, cm1 to cm7, have the ability to partially overcome OIS, whereas those within the D1 region (cm8–10, cm14–16 and cm 19–21) fail to exhibit the overcoming ability. The HBx-D5 phenotype is even found among the HBx-cm mutants (cm13, cm17 and cm18) that are defective in the coactivation function.[8] These results indicate that the ability to fully overcome OIS requires two putative functions carried by the D1 and D5 regions of the HBx protein. Because HBx-D5 does not have a positive or negative effect on RAS-induced senescence (Figs 2,3,4c), the negative regulatory domain may be active only in full-length HBx. The very low expression of HBx-D1 in human primary cells and hTERT-immortalized cells may be due to the selection result of clones, reflecting that a high level of HBx-D1 protein was eliminated due to a toxic effect of the coactivation domain,[5] or due to deletion of the N-terminal domain that has some critical role in stabilizing HBx in the expression system. Both of these may actually occur. The former is supported by the enrichment of cells expressing HBx-D1 during the early stages of drug selection. The latter is highly possible as expression levels of HBx-cm1 to HBx-cm6 covering most of the N-terminal domain were very low, as for HBx-D1. Pang *et al.* recently reported a stabilization mechanism of HBx through direct interaction with Pin1,[35] which binds phosphorylated serine and the next proline. The target serine residue is within the N-terminal domain or within the region covered by HBx-cm6. Interestingly, the HBx-cm1 to HBx-cm5 bands migrated more slowly than the HBx-cm6 band (Fig. 5b), supporting the possibility that the N-terminal domain may be critical for Pin1 binding to stabilize HBx. One interesting possibility that remains to be tested is that activation of the degradation pathway of HBx causes the toxic effect on cell proliferation. This possibility may explain the low expression of HBx-D1 and the cm mutants in the N-terminal domain. In this context, it remains unclear at present the reason for the rather stable expression of two bands of HBx-cm7 that seem to confer the same phenotype as HBx-D1 in the characterization of the cells.

The region of D1 that is responsible for overcoming RAS-induced senescence should be defined. Because some HBx-cm mutants defective in coactivation function still exhibit the ability to overcome OIS, it seems that the coactivation function is dispensable for the role. More than a dozen host factors have been reported to interact directly with the HBx-D1 region, including p53,[36,37] Smad4,[38] DDB1,[39,40] and two core subunits of the proteasome.[5] It is especially important to determine whether the binding of HBx to p53 is responsible for the ability to overcome RAS-induced senescence, as the direct binding of p53 to HBx was found to suppress p53-dependent gene activation.[5,37]

Although we have shown here that the D5 region of HBx has an indispensable biological role in anchorage-independent cell growth, the critical role of the D5 region in overcoming OIS remains obscure. The ability of the D5 region in full-length HBx

to support anchorage-independent growth will provide a good experimental system for revealing the function of the negative regulatory domain of HBx, as no host factor has been reported to interact specifically with the D5 region.

Our results clearly indicate that HBx retains the ability to overcome RAS-induced senescence in human cells immortalized by hTERT, although HBx alone could neither immortalize nor transform human cells. The ability of HBx to collaborate with active RAS in cell transformation may explain its role in hepatocellular carcinogenesis. Our findings, however, were obtained using an experimental model with immortalized cells derived from human fibroblasts. Our results may not reflect the role of HBx in HBV-infected liver, as overcoming the processes of OIS seems to vary with tissue and tumor type.[41] The role of HBx should therefore be addressed using human hepatocytes and immortalized human hepatocytes. The former, however, are quite difficult to obtain whereas the latter are available at present. It had been immortalized by introducing the other viral oncogene SV LT.[42,43]

Acknowledgments

We thank K. Masutomi and W. C. Hahn for kindly providing the retroviral vectors and human immortal cell lines, T. B. S. Yen (UCSF, USA) and H. Tang (Sichuan University, China) and the members of the Division for critical discussions, and Ms Yasukawa and Ms Kuwabara for excellent technical assistance. This work was supported in part by a Grant-in-aid for Scientific Research and Development (B) (1790031) and a Grant-in-aid for Scientific Research on Priority Areas (C) (12213050 and 17013035) from the Ministry of Education, Culture, Sports, and Technology.

References

1 Seeger C, Mason WS. Hepatitis B virus biology. *Microbiol Mol Biol Rev* 2000; **64**: 51–68.
2 Nassal M, Schaller H. Hepatitis B virus replication. *Trends Microbiol* 1993; **1**: 221–8.
3 Arbuthnot P, Kew M. Hepatitis B virus and hepatocellular carcinoma. *Int J Exp Pathol* 2001; **82**: 77–100.
4 Murakami S. Hepatitis B virus X protein: structure, function and biology. *Intervirology* 1999; **42**: 81–99.
5 Murakami S. Hepatitis B virus X protein: a multifunctional viral regulator. *J Gastroenterol* 2001; **36**: 651–60.
6 Murakami S, Cheong JH, Kaneko S. Human hepatitis virus X gene encodes a regulatory domain that represses transactivation of X protein. *J Biol Chem* 1994; **269**: 15 118–23.
7 Lin Y, Tang H, Nomura T *et al.* The hepatitis B virus X protein is a co-activator of activated transcription that modulates the transcription machinery and distal binding activators. *J Biol Chem* 1998; **273**: 27 097–103.
8 Tang H, Delgermaa L, Huang F *et al.* The transcriptional transactivation function of HBx protein is important for its augmentation role in hepatitis B virus replication. *J Virol* 2005; **79**: 5548–56.
9 Shirakata Y, Kawada M, Fujiki Y *et al.* The X gene of hepatitis B virus induced growth stimulation and tumorigenic transformation of mouse NIH3T3 cells. *Jpn J Cancer Res* 1989; **80**: 617–21.
10 Kim YC, Song KS, Yoon G *et al.* Activated ras oncogene collaborates with HBx gene of hepatitis B virus to transform cells by suppressing HBx-mediated apoptosis. *Oncogene* 2001; **20**: 16–23.
11 Kim CM, Koike K, Saito I, Miyamura T, Jay G. HBx gene of hepatitis B virus induces liver cancer in transgenic mice. *Nature* 1991; **351**: 317–20.
12 Yu DY, Moon HB, Son JK *et al.* Incidence of hepatocellular carcinoma in transgenic mice expressing the hepatitis B virus X-protein. *J Hepatol* 1999; **31**: 123–32.
13 Gottlob K, Pagano S, Levrero M, Graessmann A. Hepatitis B virus X protein transcription activation domains are neither required nor sufficient for cell transformation. *Cancer Res* 1998; **58**: 3566–70.
14 Slagle BL, Lee TH, Medina D, Finegold MJ, Butel JS. Increased sensitivity to the hepatocarcinogen diethylnitrosamine in transgenic mice carrying the hepatitis B virus X gene. *Mol Carcinog* 1996; **15**: 261–9.
15 Terradillos O, Billet O, Renard CA *et al.* The hepatitis B virus X gene potentiates c-myc-induced liver oncogenesis in transgenic mice. *Oncogene* 1997; **14**: 395–404.
16 Artandi SE, DePinho RA. Mice without telomerase: what can they teach us about human cancer? *Nat Med* 2000; **6**: 852–5.
17 Balmain A, Harris CC. Carcinogenesis in mouse and human cells: parallels and paradoxes. *Carcinogenesis* 2000; **21**: 371–7.
18 Rangarajan A, Hong SJ, Gifford A, Weinberg RA. Species- and cell type-specific requirements for cellular transformation. *Cancer Cell* 2004; **6**: 171–83.
19 Hahn WC, Counter CM, Lundberg AS, Beijersbergen RL, Brooks MW, Weinberg RA. Creation of human tumour cells with defined genetic elements. *Nature* 1999; **400**: 464–8.
20 Wei W, Jobling WA, Chen W, Hahn WC, Sedivy JM. Abolition of cyclin-dependent kinase inhibitor p16Ink4a and p21Cip1/Waf1 functions permits Ras-induced anchorage-independent growth in telomerase-immortalized human fibroblasts. *Mol Cell Biol* 2003; **23**: 2859–70.
21 Akagi T, Sasai K, Hanafusa H. Refractory nature of normal human diploid fibroblasts with respect to oncogene-mediated transformation. *Proc Natl Acad Sci USA* 2003; **100**: 13 567–72.
22 Greenberg RA, Allsopp RC, Chin L, Morin GB, DePinho RA. Expression of mouse telomerase reverse transcriptase during development, differentiation and proliferation. *Oncogene* 1998; **16**: 1723–30.
23 Newbold RF. Genetic control of telomerase and replicative senescence in human and rodent cells. *Ciba Found Symp* 1997; **211**: 177–89.
24 Harvey M, Sands AT, Weiss RS. *et al. In vitro* growth characteristics of embryo fibroblasts isolated from p53-deficient mice. *Oncogene* 1993; **8**: 2457–67.
25 Kamijo T, Zindy F, Roussel MF. *et al.* Tumor suppression at the mouse INK4a locus mediated by the alternative reading frame product p19ARF. *Cell* 1997; **91**: 649–59.
26 Sedivy JM. Can ends justify the means? Telomeres and the mechanisms of replicative senescence and immortalization in mammalian cells. *Proc Natl Acad Sci USA* 1998; **95**: 9078–81.
27 Shay JW, Wright WE, Werbin H. Defining the molecular mechanisms of human cell immortalization. *Biochim Biophys Acta* 1991; **1072**: 1–7.
28 Bodnar AG, Ouellette M, Frolkis M *et al.* Extension of life-span by introduction of telomerase into normal human cells. *Science* 1998; **279**: 349–52.
29 Halvorsen TL, Leibowitz G, Levine F. Telomerase activity is sufficient to allow transformed cells to escape from crisis. *Mol Cell Biol* 1999; **19**: 1864–70.
30 Hahn WC. Role of telomeres and telomerase in the pathogenesis of human cancer. *J Clin Oncol* 2003; **21**: 2034–43.
31 Sharpless NE, DePinho RA. Cancer: crime and punishment. *Nature* 2005; **436**: 636–7.
32 Braig M, Lee S, Loddenkemper C *et al.* Oncogene-induced senescence as an initial barrier in lymphoma development. *Nature* 2005; **436**: 660–5.
33 Hahn WC, Dessain SK, Brooks MW *et al.* Enumeration of the simian virus 40 early region elements necessary for human cell transformation. *Mol Cell Biol* 2002; **22**: 2111–23.
34 Tang H, Oishi N, Kaneko S, Murakami S. Molecular functions and biological roles of hepatitis B virus X protein. *Cancer Sci* 2006; **97**: 977–83.
35 Pang R, Lee TK, Poon RT *et al.* Pin1 interacts with a specific serine-proline motif of hepatitis B virus X-protein to enhance hepatocarcinogenesis. *Gastroenterology* 2007; **132**: 1088–1103.
36 Elmore LW, Hancock AR, Chang SF *et al.* Hepatitis B virus X protein and p53 tumor suppressor interactions in the modulation of apoptosis. *Proc Natl Acad Sci USA* 1997; **94**: 14 707–12.
37 Lin Y, Nomura T, Yamashita T, Dorjsuren D, Tang H, Murakami S. The transactivation and p53-interacting functions of hepatitis B virus X protein are mutually interfering but distinct. *Cancer Res* 1997; **57**: 5137–42.
38 Lee DK, Park SH, Yi Y *et al.* The hepatitis B virus encoded oncoprotein pX amplifies TGF-beta family signaling through direct interaction with Smad4: potential mechanism of hepatitis B virus-induced liver fibrosis. *Genes Dev* 2001; **15**: 455–66.
39 Lee TH, Elledge SJ, Butel JS. Hepatitis B virus X protein interacts with a probable cellular DNA repair protein. *J Virol* 1995; **69**: 1107–14.
40 Leupin O, Bontron S, Schaeffer C, Strubin M. Hepatitis B virus X protein stimulates viral genome replication via a DDB1-dependent pathway distinct from that leading to cell death. *J Virol* 2005; **79**: 4238–45.
41 DePinho RA. The age of cancer. *Nature* 2000; **408**: 248–54.
42 Kobayashi N, Noguchi H, Watanabe T *et al.* A new approach to develop a biohybrid artificial liver using a tightly regulated human hepatocyte cell line. *Hum Cell* 2000; **13**: 229–35.
43 Kobayashi N, Miyazaki M, Fukaya K *et al.* Treatment of surgically induced acute liver failure with transplantation of highly differentiated immortalized human hepatocytes. *Cell Transplant* 2000; **9**: 733–5.

doi: 10.1111/j.1349-7006.2007.00579.x

Tumor cell apoptosis induces tumor-specific immunity in a CC chemokine receptor 1- and 5-dependent manner in mice

Noriho Iida,* Yasunari Nakamoto,* Tomohisa Baba,† Kaheita Kakinoki,* Ying-Yi Li,† Yu Wu,† Kouji Matsushima,‡ Shuichi Kaneko,* and Naofumi Mukaida†,[1]

*Disease Control and Homeostasis, Graduate School of Medical Science, and †Division of Molecular Bioregulation, Cancer Research Institute, Kanazawa University, Kanazawa, Japan; and ‡Department of Molecular Preventive Medicine, School of Medicine, University of Tokyo, Tokyo, Japan

Abstract: The first step in the generation of tumor immunity is the migration of dendritic cells (DCs) to the apoptotic tumor, which is presumed to be mediated by various chemokines. To clarify the roles of chemokines, we induced apoptosis using suicide gene therapy and investigated the immune responses following tumor apoptosis. We injected mice with a murine hepatoma cell line, BNL 1ME A.7R.1 (BNL), transfected with HSV-thymidine kinase (tk) gene and then treated the animals with ganciclovir (GCV). GCV treatment induced massive tumor cell apoptosis accompanied with intratumoral DC infiltration. Tumor-infiltrating DCs expressed chemokine receptors CCR1 and CCR5, and T cells and macrophages expressed CCL3, a ligand for CCR1 and CCR5. Moreover, tumor apoptosis increased the numbers of DCs migrating into the draining lymph nodes and eventually generated a specific cytotoxic cell population against BNL cells. Although GCV completely eradicated HSV-tk-transfected BNL cells in CCR1-, CCR5-, or CCL3-deficient mice, intratumoral and intranodal DC infiltration and the subsequent cytotoxicity generation were attenuated in these mice. When parental cells were injected again after complete eradication of primary tumors by GCV treatment, the wild-type mice completely rejected the rechallenged cells, but the deficient mice exhibited impairment in rejection. Thus, we provide definitive evidence indicating that CCR1 and CCR5 and their ligand CCL3 play a crucial role in the regulation of intratumoral DC accumulation and the subsequent establishment of tumor immunity following induction of tumor apoptosis by suicide genes. *J. Leukoc. Biol.* 84: 1001–1010; 2008.

Key Words: *dendritic cells · gene therapy*

INTRODUCTION

Hepatocellular carcinoma (HCC) occurs in individuals with chronic liver disease related to hepatitis B or C virus infections [1–3]. Even after the curative treatments for HCC, such as surgical resection and radiofrequency ablation, tumor recurrence often occurs because of the multicentric development of HCC in the cirrhotic liver [4]. Immune-based therapies, particularly those based on dendritic cells (DCs), may be theoretically effective in preventing the recurrence because of their potential capacity to search for and eradicate tumor cells irrespective of site [5]. However, DC-based therapy is still considered to be in its infancy, probably as a result of the lack of effective techniques for enhancing the immune response to human cancer cells including HCC, which are generally poor in immunogenicity.

Apoptotic tumor cells are generally less immunogenic than necrotic cells, but they can sometimes induce efficient antitumor immune responses depending on the type of apoptosis inducer. Indeed, some anticancer drugs can induce apoptosis of tumor cells and simultaneously enhance the immunogenicity of apoptotic cancer cells [6–8]. Ganciclovir (GCV) can activate the protease family of caspases and induce apoptosis selectively in the cells transfected with the HSV-thymidine kinase (tk) gene [9, 10]. Thus, when GCV is administered systemically to tumor-bearing individuals, it induces apoptosis of HSV-tk-transfected tumor cells but not normal cells. This treatment strategy, designated as suicide gene therapy, can induce immunogenic apoptosis of the tumor cells [11], as evidenced by a massive intratumoral infiltration of macrophages and T cells [12]. Moreover, the expression of various proinflammatory cytokines is augmented at the tumor sites following GCV treatment [12, 13]. Furthermore, to enhance the suicide gene therapy-induced immune responses, the simultaneous use of cytokines such as GM-CSF, IL-2, and MCP-1/CCL2 has been used with some success [14–16]. To design more effective methods of preventing tumor recurrences, it is necessary to fully understand the immune responses after tumor apoptosis induced by HSV-tk/GCV suicide gene therapy.

DCs are potent APC that play a crucial role in the establishment of adoptive immune response. Immature DCs capture and process antigens at the inflammatory sites and thereafter migrate to the draining lymph node, where they

[1] Correspondence: Division of Molecular Bioregulation, Cancer Research Institute, Kanazawa University, 13-1 Takara-machi, Kanazawa 920-0934, Japan. E-mail: naofumim@kenroku.kanazawa-u.ac.jp

Received November 26, 2007; revised June 12, 2008; accepted June 30, 2008.

doi: 10.1189/jlb.1107791

undergo phenotypical and functional maturation. At the draining lymph node, the mature DCs interact with naïve T cells and present the captured and processed antigen to T cells [17, 18].

Chemokines are presumed to play an essential role in the regulation of DC trafficking and DC–T cell interaction in general [19–22]. Circulating immature DCs express inflammatory chemokine receptors such as CCR1, CCR2, CCR5, and CCR6, and these DCs can reach the source of the inflammatory stimulus under the guidance of the ligand gradient for the expressed receptors such as CCL2, CCL3, CCL4, CCL5, CCL7, and CCL20. After capturing antigens, DCs undergo maturation, resulting in a decrease in inflammatory chemokine receptor expression and a reciprocal increase in CCR7 expression. Mature DCs expressing CCR7 migrate to T cell-rich areas of the draining lymph nodes, where the ligands for CCR7, CCL19, and/or CCL21 are expressed abundantly. However, it still remains elusive whether similar mechanisms operate in the DC migration process following massive tumor apoptosis induced by treatments such as gene therapy, chemotherapy, and radiation therapy.

Here, we demonstrate the induction of specific tumor immunity by tumor apoptosis after HSV-tk/GCV suicide gene therapy and essential roles of DCs in this process. Moreover, we provide definitive evidence to indicate that CCR1 and CCR5 and their ligand CCL3 play a key role in the regulation of intratumoral DC accumulation and the subsequent establishment of tumor immunity following induction of tumor apoptosis by HSV-tk/GCV suicide gene therapy. These observations might lay the foundation for devising novel measures to enhance antitumor immune responses to prevent tumor recurrence.

MATERIALS AND METHODS

Mice

Specific pathogen-free, 7- to 9-week-old male BALB/c mice were purchased from Charles River Japan (Yokohama, Japan) and were designated as wild-type (WT) mice. CCL3-deficient [CCL3 knockout (CCL3KO)] mice were obtained from Jackson Laboratories (Bar Harbor, ME, USA). CCR1KO mice were a gift from Dr. Philip M. Murphy [National Institute of Allergy and Infectious Diseases, National Institutes of Health (NIAID, NIH), Bethesda, MD, USA]. CCR5KO mice were generated as described previously [23]. All mice were backcrossed to BALB/c mice for eight to 10 generations. All animal experiments were performed under specific pathogen-free conditions in accordance with the Guideline for the Care and Use of Laboratory Animals of Kanazawa University (Japan).

Tumor cell lines

A murine HCC cell line, BNL 1ME A.7R.1 (BNL), was cultured in DMEM (Sigma Chemical Co., St. Louis, MO, USA) containing 10% FBS (Gibco, Long Island, NY, USA). BNL cells were infected with the retroviral vector pG1Sv.Na harboring HSV-tk cDNA. The infected BNL cells were cultured in 10% FBS-containing DMEM in the presence of 400 μg/ml G418 (Gibco). The surviving cells were tested for sensitivity to GCV in vitro as described previously [24]. GCV-sensitive cells were designated as BNL-tk and were used in the experiments.

Apoptosis detection assay

After culturing for 1 day with 5 μg/ml GCV, BNL-tk cells were harvested, and phosphatidyl serine levels were determined by staining the cells with propidium iodide (PI) and the Annexin V-FITC apoptosis detection kit (Calbiochem, Darmstadt, Germany) according to the manufacturer's instructions. At least 50,000 stained cells were analyzed on a FACSCalibur system (BD Biosciences, San Diego, CA, USA) for each determination.

Tumor injection

Seven- to 9-week old male WT, CCR1KO, CCR5KO, and CCL3KO mice were inoculated s.c. into the left flank with 2×10^5 BNL-tk cells on Day 0. From Days 14 to 18 (5 consecutive days), 75 mg/kg GCV (i.p.) was administered daily (see **Fig. 1C**). Tumors were removed at the indicated time intervals for immunohistochemical analysis and quantitative real-time RT-PCR. In another series of experiments, WT, CCR1KO, CCR5KO, or CCL3KO mice were inoculated with 1.5×10^5 BNL-tk on Day 0. The mice were i.p.-injected with 75 mg/kg GCV from Days 2 to 5. The animals were then rechallenged s.c. with 1.0×10^5 BNL in their right flank on Day 18, after confirming that the primary tumors were eradicated completely (see Fig. 5A). Tumor sizes were evaluated twice each week using calipers, and tumor volume was calculated by the following formula: Tumor volume (mm^3) = (the longest diameter) × (the shortest diameter)^2/2.

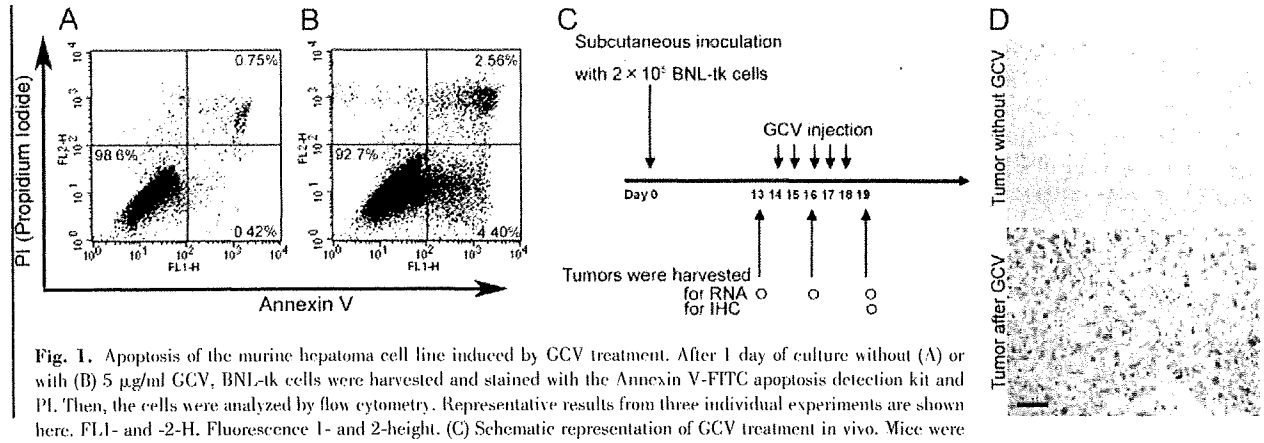

Fig. 1. Apoptosis of the murine hepatoma cell line induced by GCV treatment. After 1 day of culture without (A) or with (B) 5 μg/ml GCV, BNL-tk cells were harvested and stained with the Annexin V-FITC apoptosis detection kit and PI. Then, the cells were analyzed by flow cytometry. Representative results from three individual experiments are shown here. FL1- and -2-H, Fluorescence 1- and 2-height. (C) Schematic representation of GCV treatment in vivo. Mice were s.c.-injected with 2×10^5 BNL-tk cells on Day 0. Then, GCV was i.p.-injected into mice from Days 14 to 18. Tumors were harvested on the day before GCV injection (Day 13), on Day 3 or 6 after GCV injection (Day 16 or 19) for real-time RT-PCR analysis, and on Day 19 for immunohistochemistry (IHC). (D) Apoptotic cells detected in tumor tissues with or without GCV treatment using anti-ssDNA antibody. Original magnification, ×400. Original bar, 50 μm.

The draining lymph nodes (inguinal and axillary) were removed from the mice at the indicated time intervals for flow cytometric analysis and cytotoxicity assay.

Immunohistochemical analysis

Rabbit anti-mouse CCR5 polyclonal antibodies were prepared as described previously [25]. The removed tumor tissues were embedded in paraffin or the Sakura Tissue-Tek OCT compound (Sakura Finetek, Torrance, CA, USA) as frozen tissues. The paraffin-embedded sections were then stained with goat anti-mouse CCR1 (Santa Cruz Biotechnology, Santa Cruz, CA, USA), rabbit anti-CCR5, goat anti-mouse CCL3 (R&D Systems, Minneapolis, MN, USA), rat anti-mouse F4/80, anti-mouse CD3 (Serotec, Oxford, UK), rabbit anti-ssDNA, or rat anti-Ki67 (Dako Cytomation, Tokyo, Japan) overnight at 4°C. Cryostat sections of the frozen tissues were fixed with 4% paraformaldehyde (PFA) in PBS and stained with rat anti-mouse DEC205 (Serotec) or hamster anti-mouse CD11c (BD Biosciences) overnight at 4°C. The sections were then incubated for 1 h at room temperature with biotinylated rabbit anti-goat IgG, biotinylated swine anti-rabbit IgG, biotinylated rabbit anti-rat IgG (Dako Cytomation), or biotinylated mouse anti-hamster IgG (BD Biosciences). The immune complexes were visualized using a catalyzed signal amplification system (Dako Cytomation) or the ELITE avidin-biotin-peroxidase and diaminobenzidine substrate kits (Vector Laboratories, Burlingame, CA, USA), except for anti-ssDNA, where a novel HRP-labeled polymer (Envision$^+$, Dako Cytomation) was used, according to the manufacturer's instructions. As a negative control, goat IgG (R&D Systems), rabbit IgG (Dako Cytomation), rat IgG (Cosmo Bio, Tokyo, Japan), or hamster IgG (BD Biosciences) was used instead of specific primary antibodies. The numbers of positive cells were determined in each animal in 10 randomly chosen fields at 400-fold magnification by an examiner without any prior knowledge of the experimental procedures.

Double-color immunofluorescence analysis

Tumor tissues were embedded in paraffin or the OCT compound as frozen tissues. The paraffin-embedded sections were then stained with combinations of rat anti-mouse CD3 and goat anti-mouse CCL3 or anti-F4/80 and anti-CCL3 antibodies overnight at 4°C. After fixation with 4% PFA/PBS, cryostat sections were stained with the combinations rat anti-mouse CD4 (BD Biosciences) and anti-CCR1, rat anti-mouse CD8a (BD Biosciences) and anti-CCR1, anti-CD4 and anti-CCR5, anti-CD8a and anti-CCR5, rat anti-DEC205 and anti-CCR1, anti-DEC205 and anti-CCR5, PE-conjugated hamster anti-CD11c (BD Biosciences) and anti-CCR1, PE-conjugated anti-CD11c and anti-CCR5, PE-conjugated anti-CD11c and rat anti-CD11b (BD Biosciences), or PE-conjugated anti-CD11c and anti CD8a antibodies. After extensive washing, AF488 donkey anti-rat IgG (Invitrogen, Carlsbad, CA, USA) was applied as the secondary antibody to detect CD4-, CD8a-, CD3-, F4/80-, DEC205-, or CD11b-positive cells. Simultaneously, AF546 or AF488 donkey anti-goat IgG (Invitrogen) was used to detect CCR1- or CCL3-positive cells, and AF594 or AF488 donkey anti-rabbit IgG (Invitrogen) was used to detect CCR5-positive cells. The sections were observed using a confocal microscope (LSM 510 META, Zeiss, Thornwood, NY, USA). The percentage of double-positive cells was determined in each animal in five randomly chosen fields at 400-fold magnification by an examiner without any prior knowledge of the experimental procedures.

Flow cytometric analysis

Inguinal and axillary lymph nodes were removed and digested in a DNase I and collagenase solution (Sigma Chemical Co.). The resultant, single-cell preparations were stained with various combinations of FITC-labeled anti-CD4, FITC-labeled anti-CD86, PE-labeled anti-CD8, PE-labeled anti-CD11c, PE-labeled anti-CD44, and PE-labeled anti-CD62 ligand (CD62L) mAb (BD Biosciences). FITC-rat IgG, PE-hamster IgG, and PE-rat IgG were used as isotype controls (BD Biosciences). To prepare the tumor lysate, BNL or CT26 cells were suspended in PBS and subjected to four cycles of rapid freezing in liquid nitrogen and thawing at 55°C. The lysate was spun at 15,000 rpm to remove particulate cellular debris. To stain intracellular IFN-γ, the mononuclear cells harvested from the draining lymph nodes on Day 8 (see Fig. 5A) were incubated with the BNL or CT26 lysates at a tumor cell:mononuclear cell ratio of 1:1 in the presence of GolgiPlug (BD Biosciences). Six hours later, surface staining was performed with APC-conjugated CD8 antibodies. Intracellular IFN-γ was stained after fixation and permeabilization with BD Cytofix/Cytoperm buffer with PE-conjugated IFN-γ antibodies or isotype control using the Mouse Intracellular Cytokine Staining starter kit (BD Biosciences). At least 100,000 stained cells were analyzed on a FACSCalibur system for each determination. The data were expressed as a proportion of positive cells (compared with cells stained with an irrelevant control antibody), and the absolute positive cell numbers were calculated after determining the total cell numbers in the lymph nodes by the following formula: Absolute positive cell numbers = total cell number in the lymph nodes × percentage of positive cells × 1/100.

Quantitative real-time RT-PCR

Total RNA was extracted from the resected tumor and lymph nodes using RNA-Bee (Tel-Test, Friendswoods, TX, USA), according to the manufacturer's instructions. After the RNA preparations were further treated with RNase-free DNase I (Life Technologies, Gaithersburg, MD, USA) to remove residual DNA, cDNA was synthesized as described previously [26]. Quantitative real-time PCR was performed on an Applied Biosystems StepOne™ real-time PCR system (Applied Biosystems, Foster City, CA, USA) using the comparative threshold (C_T) quantification method. TaqMan® gene expression assays (Applied Biosystems) containing specific primers (Accession Numbers CCL3, Mm00441258_m1; CCL4, Mm00443111_m1; CCL5, Mm01302428_m1; CCR1, Mm00438260_s1; CCR5, Mm01216171_m1; GAPDH, Mm99999915_g1), TaqMan® minor groove binder probe (FAM™ dye-labeled), and TaqMan® fast universal PCR master mix were used with 10 ng cDNA to detect and quantify the expression levels of CCL3, CCL4, CCL5, CCR1, and CCR5. Reactions were performed for 20 s at 95°C and then for 40 cycles of 1 s at 95°C and 20 s at 60°C. GAPDH was amplified as an internal control. C_T values of GAPDH were subtracted from C_T values of the target genes (ΔC_T). ΔC_T values of tumors after GCV injection were compared with ΔC_T values of tumors before GCV injection.

Cytotoxicity assay

Mononuclear cells were isolated from the draining lymph nodes at the indicated time intervals and were incubated at a cell density of 2×10^6 cells/ml in the presence of 0.6×10^6 cells/ml BNL cells, which were irradiated at 50 Gy beforehand. After 5 days of culture, the cells were tested for cytotoxicity in a lactate dehydrogenase assay using the CytoTox 96 nonradioactive cytotoxicity assay kit (Promega, Madison, WI, USA), according to the manufacturer's instructions. Effector cells were added to target cells in triplicate at different E:T ratios. Percentage of specific lysis was calculated using the following formula: [(experimental−effector spontaneous−target spontaneous)/(target maximum−target spontaneous)] × 100%.

Adoptive transfer of DC

Draining lymph nodes were harvested on Day 8 (see Fig. 5A) and were digested with DNase I and collagenase solution. Mononuclear cells were obtained by centrifugation over a Histopaque-1077 density gradient (Sigma Chemical Co.), and DCs were isolated by CD11c-conjugated magnetic microbeads (Miltenyi Biotec, Auburn, CA, USA). CD11c-positive DCs (2.5×10^5/mouse) were injected into the left flank of GCV-treated KO mice on Day 8 (see Fig. 5A). On Day 18, DC-transferred mice were rechallenged with 1×10^5 BNL cells in their right flank, and tumor sizes were measured.

Statistical analysis

Data were analyzed statistically using one-way ANOVA followed by the Tukey-Kramer test, except for tumor progression data, which were analyzed using two-way ANOVA. Data of tumor sizes after adoptive transfer of the DC experiment were analyzed using the Mann-Whitney U test. $P < 0.05$ was considered statistically significant.

RESULTS

GCV treatment induces tumor cell apoptosis with intratumoral CCR1-, CCR5-, and CCL3-positive cell accumulation in WT mice

We investigated whether HSV-tk-GCV treatment can induce apoptosis in vitro in the tk-transfected murine hepatoma cell line BNL-tk. GCV treatment significantly increased the proportions of early (annexin-positive but PI-negative) and late (annexin-positive and PI-positive) apoptotic cells (Fig. 1, A and B). We injected GCV into WT mice i.p. after the s.c. BNL-tk tumor was formed macroscopically, according to the schedule, as shown in Figure 1C. Microscopic analysis revealed that more than half of the tumor cells were apoptotic and that a large number of mononuclear cells had accumulated in the tumor sites on Day 19 immediately following the completion of treatment (Fig. 1D and Supplemental Fig. 1). Thereafter, the tumor regressed macroscopically. We next investigated the chemokine receptor expression by tumor-infiltrating cells after the induction of in vivo tumor apoptosis by suicide gene therapy. Immunohistochemical analysis revealed the presence of few CCR1-, CCR5-, or CCL3-positive cells in tumors without GCV treatment (**Fig. 2A**). In contrast, GCV treatment caused intratumoral infiltration of a large number of CCR1-, CCR5-, and CCL3-positive cells in WT mice, along with massive apoptosis of tumor cells (Fig. 2A and Supplemental Fig. 2). The intratumoral mRNA expression of CCL3, CCL4, and CCL5 was markedly increased 3 days after GCV treatment, whereas that of their receptors CCR1 and CCR5 was augmented later than 3 days after GCV injection (Fig. 2B).

Tumor-infiltrating DCs express CCR1 and CCR5

To determine the type of tumor-infiltrating cells expressing CCR1, CCR5, or CCL3, we performed a double-color immunofluorescence analysis. CD4- and CD8-positive T cells expressed CCR5 but not CCR1 (**Fig. 3A** and Supplemental Fig. 3A; 78.2±8.9% of CD4-positive T cells and 92.6±8.2% of CD8-positive T cells expressed CCR5, and CCR1 was not detected in CD4- or CD8-positive T cells). In contrast, CD11c- and DEC205-positive cells, which infiltrated to tumor sites of WT mice after GCV treatment, expressed CCR1 and CCR5 (Fig. 3B and Supplemental Fig. 3B; 100% of CD11c-positive DCs expressed CCR1 and CCR5, 97.5±5.6% DEC205-positive cells expressed CCR1, and 100% DEC-positive cells expressed CCR5). Moreover, tumor-infiltrating, CD11c-positive DCs exhibited a "myeloid" phenotype, as 87.8 ± 14.8% of CD11c-positive cells expressed CD11b, and none of them expressed CD8a (Supplemental Fig. 3C). Furthermore, CCL3 proteins were detected in CD3-positive T cells, F4/80-positive macrophages (Fig. 3C; 72.0±9.1% of CD3-positive T cells and 87.0±12.0% of F4/80-positive macrophages expressed CCL3). These observations suggest that apoptosis induced by GCV treatment enhanced the expression of CCL3, CCL4, and CCL5 and then produced chemokines attracted to CD11c-positive DCs as well as CD3-positive T cells. To address this possibility, we investigated intratumoral infiltration of CD11c-positive DCs and CD3-positive T cells in CCR1KO, CCR5KO, or CCL3KO mice, which were s.c.-inoculated with 2×10^5 BNL-tk cells into WT and KO mice. The lack of CCR1, CCR5, or CCL3 had no discernible effects on the growth of primary tumors (**Fig. 4A**). Then, we injected GCV i.p. into the mice as shown in Figure 1C. Immunohistochemical analysis revealed

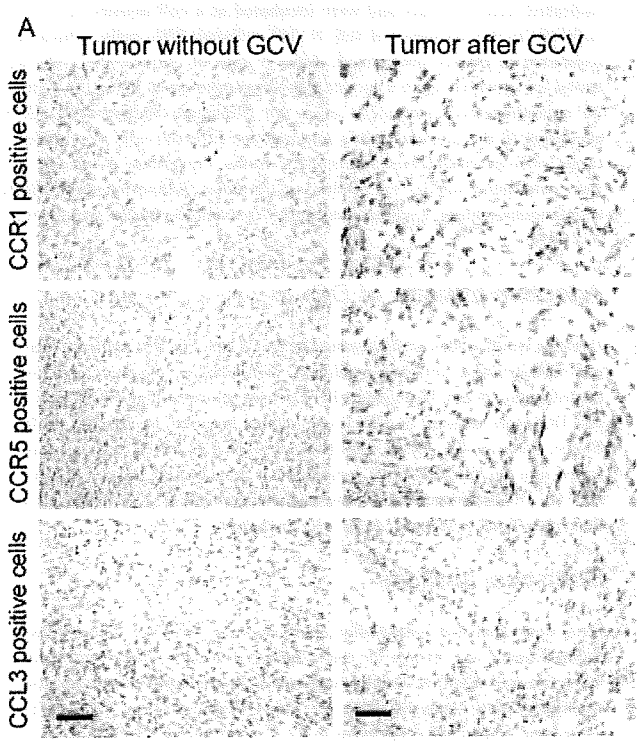

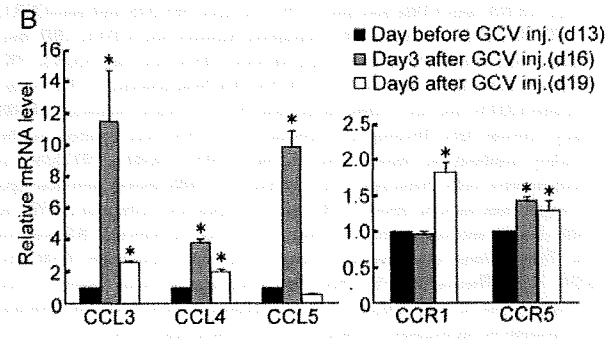

Fig. 2. Accumulation of tumor-infiltrating CCR1-, CCR5-, or CCL3-positive cells after tumor apoptosis induced by GCV treatment. Mice were inoculated with BNL-tk cells according to the schedule shown in Figure 1C. (A) Tumors were removed from WT mice on Day 19, and immunohistochemical analysis was performed using anti-CCR1, -CCR5, or -CCL3 antibody on tumors with or without GCV treatment. Representative results from three individual animals in each group are shown here. Original magnification, ×400. Original bars, 50 μm. (B) Real-time RT-PCR was performed on total RNA extracted from the tumor of WT mice harvested on Days 13, 16, or 19. The level of chemokine mRNA was normalized to GAPDH mRNA levels. Bars, ±1 SD (n=3); *, $P < 0.05$, compared with the day before GCV injection.

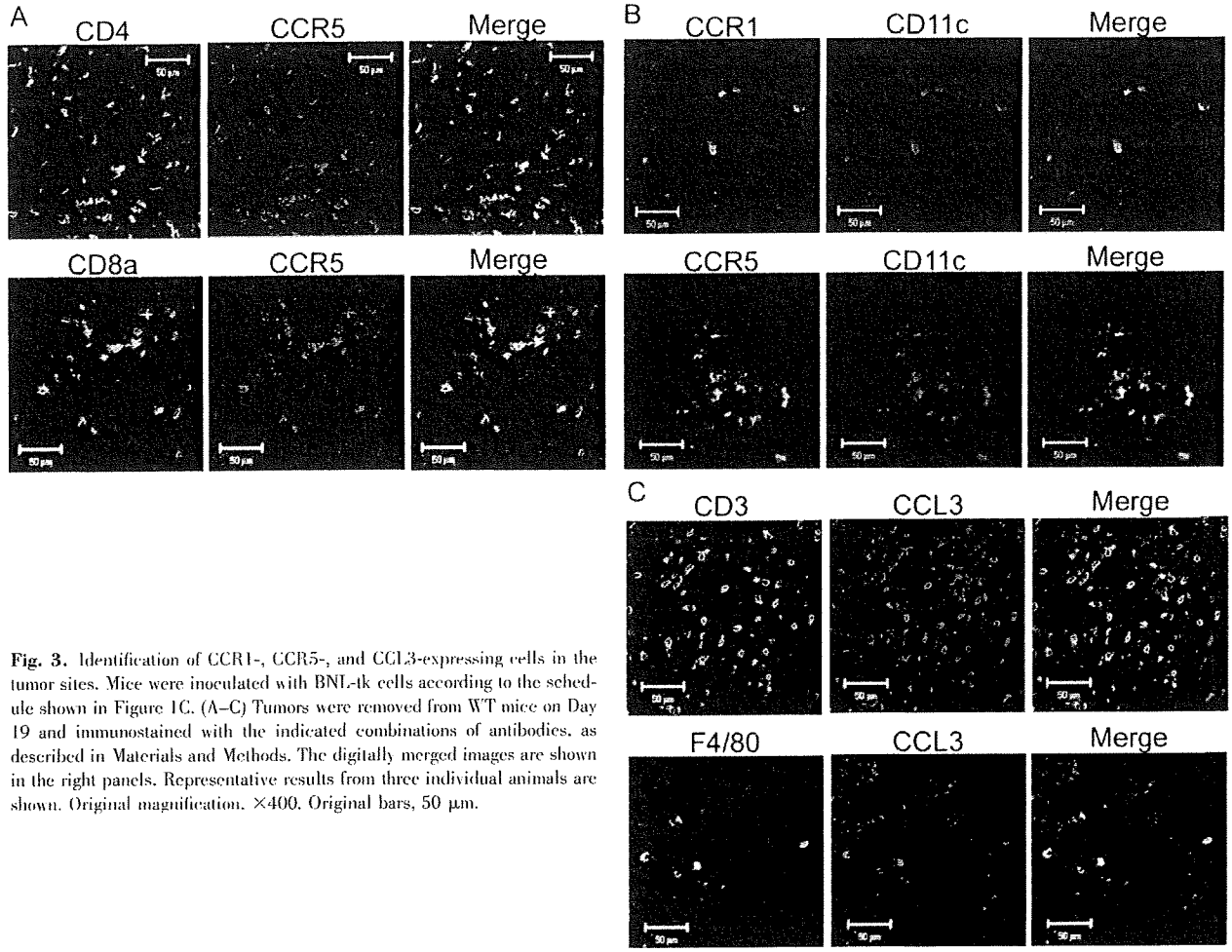

Fig. 3. Identification of CCR1-, CCR5-, and CCL3-expressing cells in the tumor sites. Mice were inoculated with BNL-tk cells according to the schedule shown in Figure 1C. (A–C) Tumors were removed from WT mice on Day 19 and immunostained with the indicated combinations of antibodies, as described in Materials and Methods. The digitally merged images are shown in the right panels. Representative results from three individual animals are shown. Original magnification, ×400. Original bars, 50 μm.

the presence of few CD3-, F4/80-, or DEC205-positive cells in tumors without GCV treatment (Fig. 4B). GCV treatment induced tumor cell apoptosis in CCL3KO, CCR1KO, and CCR5KO mice to a similar extent as that in WT mice (data not shown). Moreover, GCV treatment caused intratumoral accumulation of a large number of CD3-, CD4-, and CD8-positive T cells and DEC205- and CD11c-positive DCs in WT mice (Fig. 4, B and C). By contrast, the increases in intratumorally accumulating DEC205- and CD11c-positive cells and to a lesser extent, CD3-, CD4-, and CD8-positive cells were attenuated in CCR1KO, CCR5KO, and CCL3KO mice (Fig. 4, B and C). In contrast, GCV treatment induced intratumoral infiltration of F4/80-positive macrophages (Fig. 4B) and CD49b/DX5-positive NK cells (data not shown) in WT and KO mice to a similar extent.

Partial failure of CCR1KO, CCR5KO, and CCL3KO mice in rejecting the rechallenged tumor

Apoptosis induced by GCV treatment caused intratumoral infiltration of DCs and T cells in a CCR1- and/or CCR5-dependent manner. As intratumoral infiltration of DCs and T cells is a prerequisite for the establishment of specific tumor immunity, we examined the immune status of GCV-treated mice by rechallenging the parental BNL cell line. To completely eradicate the primary BNL-tk tumor, GCV was administered between 2 and 5 days after the tumor injection (**Fig. 5A**). Primary BNL-tk tumors were eradicated completely in WT, CCR1KO, CCR5KO, and CCL3KO mice at similar rates (data not shown). When these mice were injected again with parental BNL cells, WT mice rejected them completely. In contrast, CCR1KO, CCR5KO, and CCL3KO mice failed to completely eliminate the rechallenged tumor cells, although the growth rates were retarded in these mice compared with naïve WT mice (Fig. 5B). A marked cytotoxicity against BNL but not in CT26 cells was observed when draining lymph node-derived mononuclear cells of GCV-treated WT mice were used as effector cells. Only a modest amount of cytotoxicity was detected when mononuclear cells in the draining lymph nodes of GCV-treated CCR1KO, CCR5KO, or CCL3KO mice were used as effector cells (Fig. 5C). Further, GCV-induced tumor apoptosis enhanced the mRNA expression of Th1 cytokines such as IFN-γ, IL-12p40, and IL-18 in the draining lymph nodes of WT mice but not of CCR1KO, CCR5KO, and CCL3KO mice (Supplemental Fig. 4). Likewise, $CD8^+IFN\text{-}\gamma^+$ cells were increased markedly in GCV-treated WT mice when lymph node-derived mononuclear cells were cocultured with BNL cell lysates, compared with tumor-bearing or tumor-free

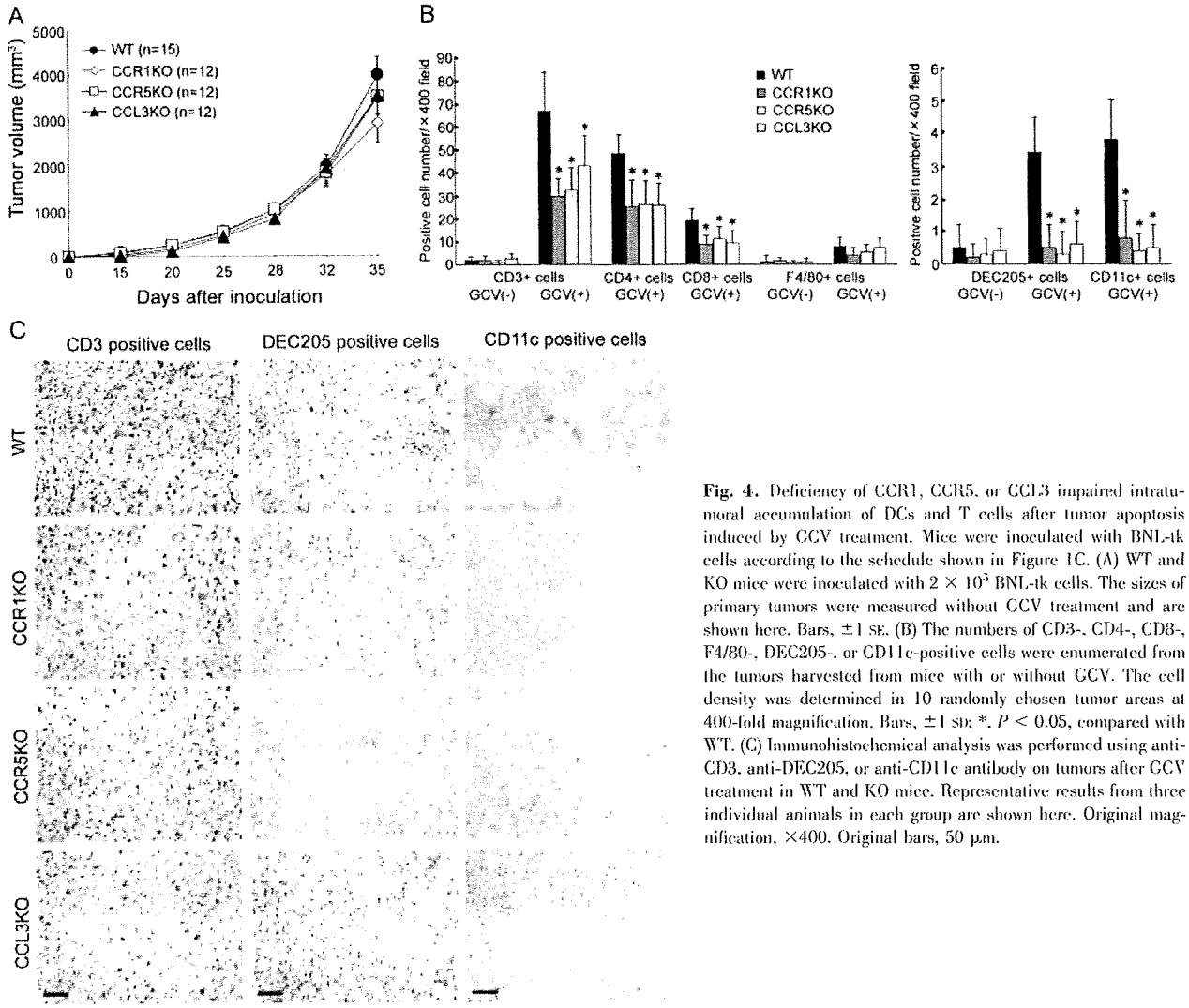

Fig. 4. Deficiency of CCR1, CCR5, or CCL3 impaired intratumoral accumulation of DCs and T cells after tumor apoptosis induced by GCV treatment. Mice were inoculated with BNL-tk cells according to the schedule shown in Figure 1C. (A) WT and KO mice were inoculated with 2×10^5 BNL-tk cells. The sizes of primary tumors were measured without GCV treatment and are shown here. Bars, ±1 SE. (B) The numbers of CD3-, CD4-, CD8-, F4/80-, DEC205-, or CD11c-positive cells were enumerated from the tumors harvested from mice with or without GCV. The cell density was determined in 10 randomly chosen tumor areas at 400-fold magnification. Bars, ±1 SD; *, $P < 0.05$, compared with WT. (C) Immunohistochemical analysis was performed using anti-CD3, anti-DEC205, or anti-CD11c antibody on tumors after GCV treatment in WT and KO mice. Representative results from three individual animals in each group are shown here. Original magnification, ×400. Original bars, 50 μm.

WT mice (Fig. 5D). Increases in $CD8^+IFN\text{-}\gamma^+$ cells were less evident in CCR1KO, CCR5KO, or CCL3KO mice treated with tumor cells and GCV compared with WT mice when lymph node-derived cells were cocultured with BNL cell lysates (Fig. 5D). These observations suggest that the absence of CCR1, CCR5, or CCL3 greatly impaired the apoptosis-induced establishment of specific tumor immunity.

Apoptosis-induced migration of DCs to draining lymph nodes and intranodal T cell proliferation activation in a CCR1-, CCR5-, and/or CCL3-dependent manner

Tumor-infiltrating DCs can uptake tumor antigens at the tumor sites and migrate to the draining lymph nodes, where they mature to present antigens to T cells [17, 18]. Thus, we further explored the status of DCs as well as T cells in the draining lymph nodes. Following GCV treatment, tumor apoptosis increased the proportions of $CD86^+CD11c^+$ cells in the draining lymph nodes but not in distant lymph nodes in WT mice (**Fig. 6A**). In contrast, GCV-induced increases in $CD11c^+$ cell proportion were depressed in CCR1KO, CCR5KO, or CCL3KO mice (Fig. 6A). The levels of CD86 on $CD11c^+$ cells were increased in GCV-treated WT mice compared with WT mice, which had been injected with neither BNL-tk cells nor GCV, although the levels of CD86 were depressed in the KO mice (mean fluorescent intensities of CD86 on $CD11c^+$ cells: WT/BNL-tk/GCV, 114.3±8.6; WT/BNL-tk, 86.2±12.2; WT/no tumor, 86.5±2.6; CCR1KO/BNL-tk/GCV, 85.4±15.6; CCR5KO/BNL-tk/GCV, 92.3±12.6; CCL3KO/BNL-tk/GCV, 79.0±9.8). Moreover, GCV-induced tumor apoptosis significantly increased the numbers of total cells, $CD4^+$ and $CD8^+$ cells, in the draining lymph nodes of WT mice. GCV-induced increases in these cell populations were also attenuated in CCR1KO, CCR5KO, or CCL3KO mice (Fig. 6B). Lymphocytes expressing the cell proliferation marker Ki67 were increased in the paracortical areas of the draining lymph nodes of GCV-treated WT mice compared with the other groups (Fig. 6C and Supplemental Fig. 5). Injection of BNL-tk cells marginally increased the proportion of activated $CD4^+$ T cells, defined as $CD44^{hi}CD62L^{lo}CD4^+$, in the draining lymph nodes. Coinjec-

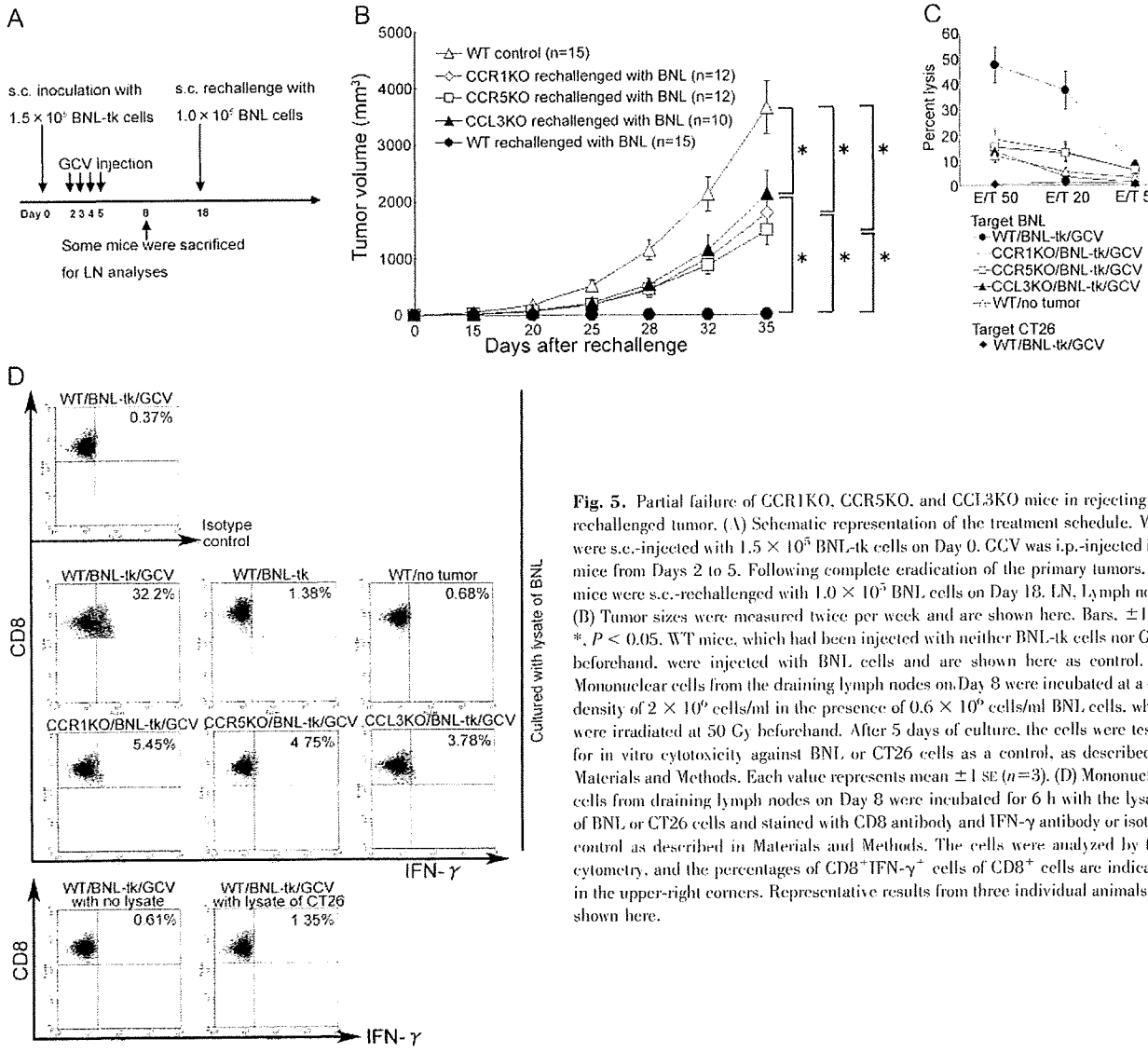

Fig. 5. Partial failure of CCR1KO, CCR5KO, and CCL3KO mice in rejecting the rechallenged tumor. (A) Schematic representation of the treatment schedule. Mice were s.c.-injected with 1.5×10^5 BNL-tk cells on Day 0. GCV was i.p.-injected into mice from Days 2 to 5. Following complete eradication of the primary tumors, the mice were s.c.-rechallenged with 1.0×10^6 BNL cells on Day 18. LN, Lymph node. (B) Tumor sizes were measured twice per week and are shown here. Bars, ±1 SE; *, $P < 0.05$. WT mice, which had been injected with neither BNL-tk cells nor GCV beforehand, were injected with BNL cells and are shown here as control. (C) Mononuclear cells from the draining lymph nodes on Day 8 were incubated at a cell density of 2×10^6 cells/ml in the presence of 0.6×10^6 cells/ml BNL cells, which were irradiated at 50 Gy beforehand. After 5 days of culture, the cells were tested for in vitro cytotoxicity against BNL or CT26 cells as a control, as described in Materials and Methods. Each value represents mean ±1 SE ($n=3$). (D) Mononuclear cells from draining lymph nodes on Day 8 were incubated for 6 h with the lysates of BNL or CT26 cells and stained with CD8 antibody and IFN-γ antibody or isotype control as described in Materials and Methods. The cells were analyzed by flow cytometry, and the percentages of $CD8^+IFN\text{-}\gamma^+$ cells of $CD8^+$ cells are indicated in the upper-right corners. Representative results from three individual animals are shown here.

tion of GCV further augmented this increment in WT mice but not in KO mice (Fig. 6, D and E). These observations suggest that the absence of CCR1, CCR5, or CCL3 impaired the GCV-induced migration of DCs into the draining lymph nodes and the subsequent proliferation and activation of T cells in the draining lymph nodes.

Restoration of anti-tumor response of KO mice by adoptive transfer of DCs harvested from GCV-treated WT mice

Given the proposed, crucial role of DCs in evoking antitumor immunity after tumor apoptosis, we finally performed adoptive transfer of DCs harvested from the draining lymph nodes of GCV-treated WT mice into the KO mice. DCs were harvested from the draining lymph nodes of GCV-treated, tumor-bearing or tumor-free WT mice and were transferred s.c. into the KO mice on Day 8 (Fig. 5A). The KO mice completely rejected the rechallenged cells when DCs were transferred from GCV-treated, tumor-bearing WT mice but not tumor-free WT mice (**Fig. 7**). These observations suggest that GCV-induced tumor apoptosis mediated the trafficking of DCs to the draining lymph nodes, which can induce the establishment of specific immunity in a CCR1-, CCR5-, or CCL3-dependent manner.

DISCUSSION

Apoptosis was previously presumed to be immunologically silent or even tolerogenic [27]. However, recent reports have indicated that tumor cell apoptosis can induce antitumor immune responses effectively, as the immunogenicity of apoptotic tumor cells is dependent on apoptosis inducers. Indeed, gemcitabine-induced apoptosis can augment cross-priming of tumor-specific $CD8^+$ T cells in vivo rather than cross-tolerizing [8]. Similarly, apoptosis induced by local radiation therapy can generate tumor antigen-specific effector cells that migrate to

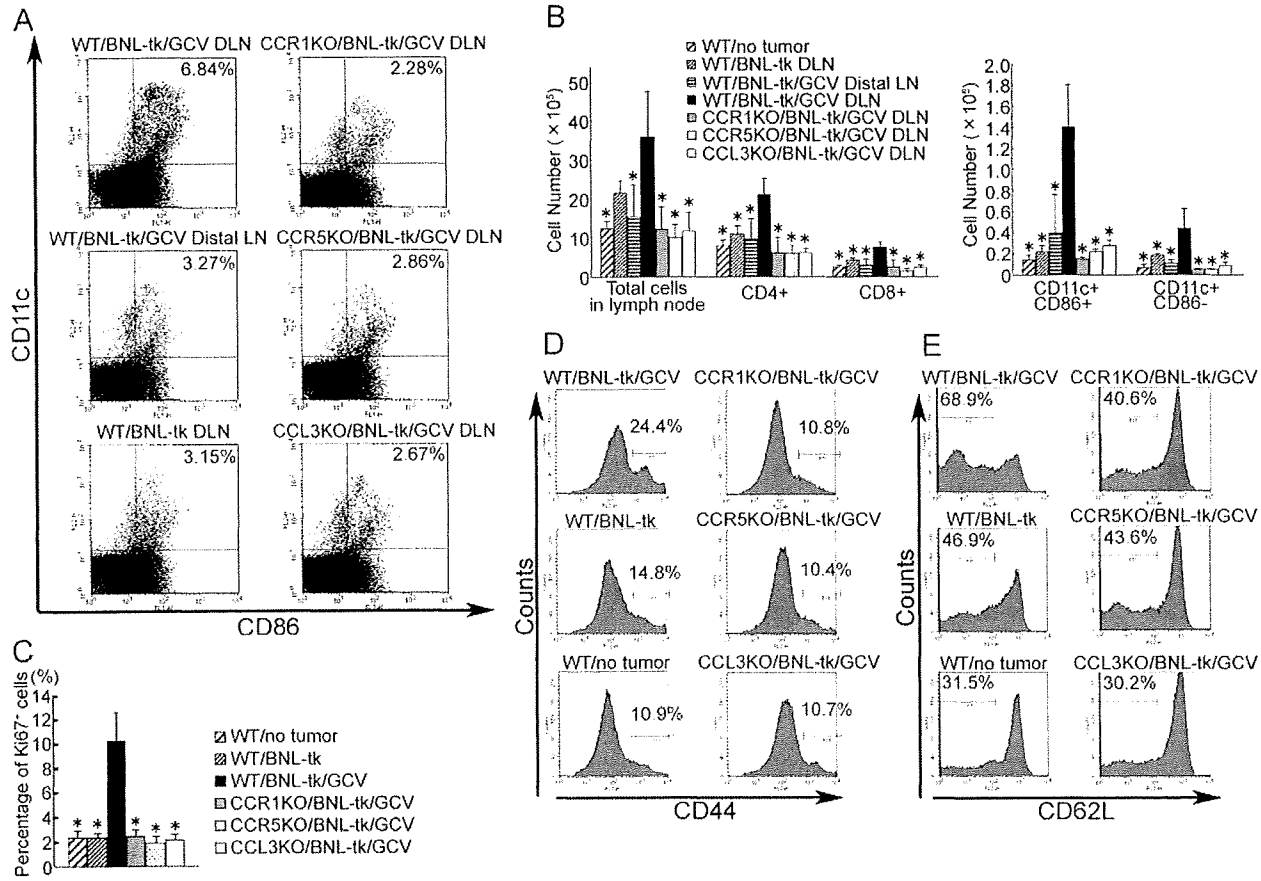

Fig. 6. Apoptosis-induced migration of DCs to the draining lymph nodes (DLN) and intranodal T cell proliferation and activation in a CCR1-, CCR5-, and/or CCL3-dependent manner. Mice were treated according to the schedule shown in Figure 5A. (A) Draining lymph nodes or distal lymph nodes were harvested on Day 8 as indicated in Figure 5A. Mononuclear cells were stained with a combination of FITC-labeled anti-CD86 and PE-labeled anti-CD11c antibodies. The percentage of $CD11c^+CD86^+$ cells was determined and is indicated in the upper-right corners. Representative results from three individual animals are shown here. (B) Absolute cell numbers of each cell population in the draining lymph nodes or distal lymph nodes on Day 8 were determined as described in Materials and Methods. Error bars, ±1 SD; *, $P < 0.05$, compared with draining lymph nodes derived from WT mice treated with BNL-tk/GCV. (C) Draining lymph nodes harvested on Day 8 were immunostained with anti-Ki67 antibody, and percentages of $Ki67^-$ cells in lymph nodes were determined. Error bars, ±1 SD; *, $P < 0.05$, compared with draining lymph nodes derived from WT mice treated with BNL-tk/GCV. (D and E) Mononuclear cells harvested on Day 8 were stained with a combination of FITC-labeled anti-CD4 and PE-labeled anti-CD44 (D) or PE-labeled anti-CD62L (E) antibodies. Histograms were gated on CD4-positive cells, and percentages of $CD44^{hi}$ (D) or $CD62L^{lo}$ (E) cells were determined. Representative results from three individual animals are shown here.

the tumor [28]. Moreover, apoptotic change caused by anthracyclin can induce the translocation of calreticulin to the apoptotic tumor cell surface, and calreticulin exposure can enhance the immunogenicity of apoptotic cancer cells [6, 7]. Thus, apoptosis induced by these measures is sufficiently immunogenic to prevent tumor progression.

The combination of HSV-tk gene transfer and GCV can efficiently induce the apoptosis of the transfected tumors as observed in the present study. Here, we also observed that the treatment augmented the immune response, as evidenced by an increase in the number of tumor-infiltrating DCs. Subsequently, the number of DCs in the draining lymph nodes increased together with enhanced, specific immunity to the injected tumor. These observations suggest that tumor apoptosis induced by HSV-tk/GCV treatment is effective in generating specific tumor immunity, similar to that observed in the case of anticancer drug treatment.

Consistent with our present observations, CCL3 and its related chemokine CCL5 were detected in macrophages infiltrating human cancer tissues [29, 30]. Given their potent chemotactic activity against various types of immune cells [31], gene transfer of CCL3 or CCL5 induced the accumulation of immune cells including DCs, T cells, macrophages, and NK cells in the tumor sites, resulting in delayed tumor growth and prolonged survival [16, 32–34]. Moreover, combination therapy of the HSV-tk and CCL3/CCL20 gene induces an exaggerated accumulation of DCs, $CD4^+$ cells, $CD8^+$ cells, NK cells, and macrophages in the tumor sites compared with HSV-tk/GCV treatment alone, and the net effects are tumor regression and prolonged survival [34]. However, the roles of endogenously produced CCL3 and its related chemokines in tumor apoptosis still remain to be elucidated.

In human HCC, tumor-infiltrating lymphocytes express high levels of CCR5 and CXCR3. Moreover, these lymphocytes

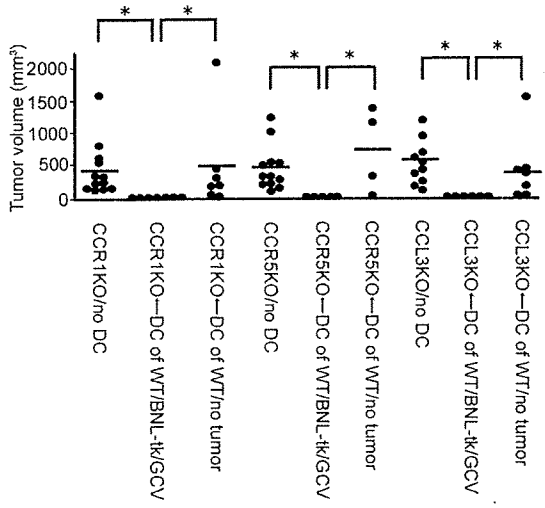

Fig. 7. Adoptive transfer of DCs harvested from GCV-treated WT mice restored the antitumor response of KO mice. After inoculation of BNL-tk tumors, CCR1KO, CCR5KO, or CCL3KO mice were treated with GCV from Days 2 to 5 as described in Figure 5A. The DCs were then harvested from the draining lymph nodes of GCV-treated WT mice and transferred s.c. into the KO mice on Day 8 as shown in Figure 5A. On Day 18, these mice were injected again with parental BNL cells, and tumor sizes were measured on Day 28. GCV-treated KO mice, transferred without or with DCs of naïve WT mice, were also rechallenged with parental BNL cells as control. Bars, mean; *, $P < 0.05$.

show strong chemotactic responses to CC and CXC chemokines including CCL3, CCL4, and CXCL9 [35]. Additional treatments are nevertheless required to enhance the immune responses, as the CCR5- or CXCR3-positive lymphocytes are insufficient to evoke immune responses and eradicate tumor tissues. We demonstrated that suicide gene therapy-induced tumor cell apoptosis augments CCR1- and CCR5-positive cell infiltration into the hepatoma tissues. Further, these CCR1- or CCR5-positive cells are DCs and/or T cells—the cells indispensable for tumor immunity. Thus, suicide gene therapy can potentially enhance tumor immunity by attracting these immune cells to the apoptotic tumor cells.

The initial step leading to specific tumor immunity is the capture of tumor antigens by macrophages and immature DCs, both of which accumulate in tumor sites. However, in this model, CCR1KO, CCR5KO, and CCL3KO mice failed to completely eliminate the rechallenged tumor cells along with reduced intratumoral accumulation of DCs but not F4/80-positive macrophages. These observations suggest that the establishment of specific tumor immunity requires intratumoral recruitment of immature DCs but not macrophages. Activated NK cells can also induce DC maturation in lymphoid organs as well as in nonlymphoid tissues. Although NK cells express chemokine receptors such as CCR5 [36], the deficiency of CCR1 or CCR5 has little effects on intratumoral infiltration of NK cells. These observations preclude the crucial role of NK cells in the establishment of specific tumor immunity in this model.

Immature DCs use several chemokine receptors including CCR1, CCR2, CCR4, CCR5, CCR6, CCR8, and CXCR4 for their migration [22]. However, the chemokine receptor(s) regulating immature DC trafficking to tumor sites still need(s) to be determined. We previously observed that CCL3 induced mobilization of DC precursors into circulation [37] and detected CCL3 in tumor-infiltrating $CD3^+$ T cells and macrophages after GCV treatment. Therefore, we investigated the roles of CCL3 and its receptors CCR1 and CCR5 in the intratumoral recruitment of DCs and the subsequent establishment of specific tumor immunity. Although CCL4 and CCL5 expression was augmented along with CCL3 expression in tumor sites, the deletion of the *CCL3* gene alone markedly reduced the DC migration, intranodal T cell accumulation, and subsequent Th1 cytokine expression. Similarly, deletion of the *CCL3* gene alone prevented coxsackievirus-induced myocarditis [38], despite enhanced, intracardiac expression of CCL3, CCL4, and CCL5 mRNA [39]. Thus, these three chemokines may form a positive feedback loop, and the deletion of either chemokine might reduce the expression of the others. Moreover, the lack of CCR1 or CCR5 reduces the migration of DCs to tumor sites and subsequent tumor immunity in the draining lymph nodes, such as DC and T cell accumulation and Th1 cytokine expression. As almost all CD11c- and DEC205-positive DCs express CCR1 and CCR5, DC migration may require coordinated and synergistic actions of both of these chemokine receptors.

We have provided definitive evidence regarding the essential contribution of CCL3 and its receptors to apoptosis-induced, specific tumor immunity, which exert their role by attracting DCs to tumor tissues. These observations further suggest that specific tumor immunity can be established more efficiently if some techniques such as chemokine gene transfer can augment the recruitment of immature DCs to apoptotic tumor tissues caused by chemotherapeutic agents and/or irradiation as well as suicide gene therapy.

ACKNOWLEDGMENTS

We thank Dr. Philip M. Murphy (NIAID, NIH) for providing us with CCR1KO mice. We also thank Dr. Toshikazu Kondo (Wakayama Medical University, Wakayama, Japan) for his technical advice about double-color immunofluorescence analysis.

REFERENCES

1. Tsukuma, H., Hiyama, T., Tanaka, S., Nakao, M., Yabuuchi, T., Kitamura, T., Nakanishi, K., Fujimoto, I., Inoue, A., Yamazaki, H., Kawashima, T. (1993) Risk factors for hepatocellular carcinoma among patients with chronic liver disease. *N. Engl. J. Med.* **328,** 1797–1801.
2. Velázquez, R. F., Rodríguez, M., Navascués, C. A., Linares, A., Pérez, R., Sotorríos, N. G., Martínez, I., Rodrigo, L. (2003) Prospective analysis of risk factors for hepatocellular carcinoma in patients with liver cirrhosis. *Hepatology.* **37,** 520–527.
3. Okita, K. (2006) Management of hepatocellular carcinoma in Japan. *J. Gastroenterol.* **41,** 100–106.
4. Poon, R. T., Fan, S. T., Ng, I. O., Lo, C. M., Liu, C. L., Wong, J. (2000) Different risk factors and prognosis for early and late intrahepatic recurrence after resection of hepatocellular carcinoma. *Cancer* **89,** 500–507.
5. Butterfield, L. H. (2004) Immunotherapeutic strategy for hepatocellular carcinoma. *Gastroenterology* **127,** S232–S241.
6. Obeid, M., Tesniere, A., Ghiringhelli, F., Fimia, G. M., Apetoh, L., Perfettini, J. L., Castedo, M., Mignot, G., Panaretakis, T., Casares, N.,

Métivier, D., Larochette, N., van Endert, P., Ciccosanti, F., Piacentini, M., Zitvogel, L., Kroemer, G. (2007) Calreticulin exposure dictates the immunogenicity of cancer cell death. *Nat. Med.* **13,** 54–61.
7. Casares, N., Pequignot, M. O., Tesniere, A., Chiringhelli, F., Roux, S., Chaput, N., Schmitt, E., Hamai, A., Hervas-Stubbs, S., Obeid, M., Coutant, F., Métivier, D., Pichard, E., Aucouturier, P., Pierron, G., Garrido, C., Zitvogel, L., Kroemer, G. (2005) Caspase-dependent immunogenicity of doxorubicin-induced tumor cell death. *J. Exp. Med.* **202,** 1691–1701.
8. Nowak, A. K., Lake, R. A., Marzo, A. L., Scott, B., Heath, W. R., Collins, E. J., Frelinger, J. A., Robinson, B. W. S. (2003) Induction of tumor cell apoptosis in vivo increases tumor antigen cross-presentation, cross-priming rather than cross-tolerizing host tumor-specific CD8 T cells. *J. Immunol.* **170,** 4905–4913.
9. Hamel, W., Magnelli, L., Chiarugi, V. P., Israel, M. A. (1996) Herpes simplex virus thymidine kinase/ganciclovir-mediated apoptotic death of bystander cells. *Cancer Res.* **56,** 2697–2702.
10. Beltinger, C., Fulda, S., Kammertoens, T., Meyer, E., Uckert, W., Debatin, K. M. (1999) Herpes simplex virus thymidine kinase/ganciclovir-induced apoptosis involves ligand-independent death receptor aggregation and activation of caspases. *Proc. Natl. Acad. Sci. USA* **96,** 8699–8704.
11. Freeman, S. M., Ramesh, R., Marrogi, A. J. (1997) Immune system in suicide-gene therapy. *Lancet* **349,** 2–3.
12. Vile, R. G., Castleden, S., Marshall, J., Camplejohn, R., Upton, C., Chong, H. (1997) Generation of an anti-tumor immune response in a non-immunogenic tumor: HSVtk killing in vivo stimulates a mononuclear cell infiltrate and a Th1-like profile of intratumoural cytokine expression. *Int. J. Cancer* **71,** 267–274.
13. Freeman, S. M., Ramesh, R., Shastri, M., Munshi, A., Jensen, A. K., Marrogi, A. J. (1995) The role of cytokines in mediating the bystander effect using HSV-TK xenogeneic cells. *Cancer Lett.* **92,** 167–174.
14. Chen, S. H., Chen, X. H. L., Wang, Y., Kosai, K., Finegold, M. J., Rich, S. S., Woo, S. L. C. (1995) Combination gene therapy for liver metastasis of colon carcinoma in vivo. *Proc. Natl. Acad. Sci. USA* **92,** 2577–2581.
15. Chen, S. H., Kosai, K., Xu, B., Pham-Nguyen, K., Contant, C., Finegold, M. J., Woo, S. L. C. (1996) Combination suicide and cytokine gene therapy for hepatic metastases of colon carcinoma: sustained antitumor immunity prolongs animal survival. *Cancer Res.* **56,** 3758–3762.
16. Tsuchiyama, T., Nakamoto, Y., Sakai, Y., Marukawa, Y., Kitahara, M., Mukaida, N., Kaneko, S. (2007) Prolonged, NK cell-mediated antitumor effects of suicide gene therapy combined with monocyte chemoattractant protein-1 against hepatocellular carcinoma. *J. Immunol.* **178,** 574–583.
17. Banchereau, J., Steinman, R. M. (1998) Dendritic cells and the control of immunity. *Nature* **392,** 245–252.
18. Sallusto, F., Lanzavecchia, A. (1999) Mobilizing dendritic cells for tolerance, priming, and chronic inflammation. *J. Exp. Med.* **189,** 611–614.
19. Castellino, F., Huang, A. Y., Altan-Bonnet, G., Stoll, S., Scheinecker, C., Germain, R. N. (2006) Chemokines enhance immunity by guiding naïve $CD8^+$ T cells to sites of $CD4^+$ T cell-dendritic cell interaction. *Nature* **440,** 890–895.
20. Dieu, M. C., Vanbervliet, B., Vicari, A., Bridon, J. M., Oldham, E., Aït-Yahia, S., Brière, F., Zlotnik, A., Lebecque, S., Caux, C. (1998) Selective recruitment of immature and mature dendritic cells by distinct chemokines expressed in different anatomic sites. *J. Exp. Med.* **188,** 373–386.
21. Sozzani, S., Luini, W., Borsatti, A., Polentarutti, N., Zhou, D., Piemonti, L., D'Amico, G., Power, C. A., Wells, T. N. C., Gobbi, M., Allavena, P., Mantovani, A. (1997) Receptor expression and responsiveness of human dendritic cells to a defined set of CC and CXC chemokines. *J. Immunol.* **159,** 1993–2000.
22. Sozzani, S. (2005) Dendritic cell trafficking: more than just chemokines. *Cytokine Growth Factor Rev.* **16,** 581–592.
23. Murai, M., Yoneyama, H., Ezaki, T., Suematsu, M., Terashima, Y., Harada, A., Hamada, H., Asakura, H., Ishikawa, H., Matsushima, K. (2003) Peyer's patch is the essential site in initiating murine acute and lethal graft-versus-host reaction. *Nat. Immunol.* **4,** 154–160.
24. Tsuchiyama, T., Kaneko, S., Nakamoto, Y., Sakai, Y., Honda, M., Mukaida, N., Kobayashi, K. (2003) Enhanced antitumor effects of a bicistronic adenovirus vector expressing both herpes simplex virus thymidine kinase and monocyte chemoattractant protein-1 against hepatocellular carcinoma. *Cancer Gene Ther.* **10,** 260–269.
25. Murai, M., Yoneyama, H., Harada, A., Yi, Z., Vestergaard, C., Guo, B., Suzuki, K., Asakura, H., Matsushima, K. (1999) Active participation of $CCR5^+CD8^+$ T lymphocytes in the pathogenesis of liver injury in graft-versus-host disease. *J. Clin. Invest.* **104,** 49–57.
26. Lu, P., Nakamoto, Y., Nemoto-Sakai, Y., Fujii, C., Wang, H., Hashii, M., Ohmoto, Y., Kaneko, S., Kobayashi, K., Mukaida, N. (2003) Potential interaction between CCR1 and its ligand, CCL3, induced by endogeneously produced interleukin-1 in human hepatomas. *Am. J. Pathol.* **162,** 1249–1258.
27. Steinman, R. M., Turley, S., Mellman, I., Inaba, K. (2000) The induction of tolerance by dendritic cells that have captured apoptotic cells. *J. Exp. Med.* **191,** 411–416.
28. Lugade, A. A., Moran, J. P., Gerber, S. A., Rose, R. C., Frelinger, J. G., Lord, E. M. (2005) Local radiation therapy of B16 melanoma tumors increases the generation of tumor antigen-specific effector cells that traffic to the tumor. *J. Immunol.* **174,** 7516–7523.
29. Tang, K. F., Tan, S. Y., Chan, S. H., Chong, S. M., Loh, K. S., Tan, L. K. S., Hu, H. (2001) A distinct expression of CC chemokines by macrophages in nasopharyngeal carcinoma: implication for the intense tumor infiltration by T lymphocytes and macrophages. *Hum. Pathol.* **32,** 42–49.
30. Musha, H., Ohtani, H., Mizoi, T., Kinouchi, M., Nakayama, T., Shiiba, K., Miyagawa, K., Nagura, H., Yoshie, O., Sasaki, I. (2005) Selective infiltration of $CCR5^+CXCR3^+$ T lymphocytes in human colorectal carcinoma. *Int. J. Cancer* **116,** 949–956.
31. Menten, P., Wuyts, A., van Damme, J. (2002) Macrophage inflammatory protein-1. *Cytokine Growth Factor Rev.* **13,** 455–481.
32. Lavergne, E., Combadière, C., Iga, M., Boissonnas, A., Bonduelle, O., Maho, M., Debré, P., Combadiere, B. (2004) Intratumoral CC chemokine ligand 5 overexpression delays tumor growth and increases tumor cell infiltration. *J. Immunol.* **173,** 3755–3762.
33. Fushimi, T., Kojima, A., Moore, M. A., Crystal, R. G. (2000) Macrophage inflammatory protein 3α transgene attracts dendritic cells to established murine tumors and suppresses tumor growth. *J. Clin. Invest.* **105,** 1383–1393.
34. Crittenden, M., Cough, M., Harrington, K., Olivier, K., Thompson, J., Vile, R. G. (2003) Expression of inflammatory chemokines combined with local tumor destruction enhances tumor regression and long-term immunity. *Cancer Res.* **63,** 5505–5512.
35. Yoong, K. F., Afford, S. C., Jones, R., Aujla, P., Qin, S., Price, K., Hubscher, S. G., Adams, D. H. (1999) Expression of CXC and CC chemokines in human malignant liver tumors: a role for human monokine induced by γ-interferon in lymphocyte recruitment to hepatocellular carcinoma. *Hepatology* **30,** 100–111.
36. Walzer, T., Dalod, M., Robbins, S. H., Zitvogel, L., Vivier, E. (2005) Natural-killer cells and dendritic cells: "l'union fait la force". *Blood* **106,** 2252–2258.
37. Zhang, Y., Yoneyama, H., Wang, Y., Ishikawa, S., Hashimoto, S., Gao, J. L., Murphy, P. M., Matsushima, K. (2004) Mobilization of dendritic cell precursors into the circulation by administration of MIP-1α in mice. *J. Natl. Cancer Inst.* **96,** 201–209.
38. Cook, D. N., Beck, M. A., Coffman, T. M., Kirby, S. L., Sheridan, J. F., Pragnell, I. B., Smithies, O. (1995) Requirement for an inflammatory response to viral infection. *Science* **269,** 1583–1585.
39. Gebhard, J. R., Perry, C. M., Harkins, S., Lane, T., Mena, I., Asensio, V. C., Campbell, I. L., Whitton, J. L. (1998) Coxsackievirus B3-induced myocarditis. Perforin exacerbates disease, but plays no detectable role in virus clearance. *Am. J. Pathol.* **153,** 417–428.

Common Transcriptional Signature of Tumor-Infiltrating Mononuclear Inflammatory Cells and Peripheral Blood Mononuclear Cells in Hepatocellular Carcinoma Patients

Yoshio Sakai, Masao Honda, Haruo Fujinaga, Isamu Tatsumi, Eishiro Mizukoshi, Yasunari Nakamoto, and Shuichi Kaneko

Department of Gastroenterology, Kanazawa University, School of Medicine, Kanazawa, Japan

Abstract

Hepatocellular carcinoma (HCC) is frequently associated with infiltrating mononuclear inflammatory cells. We performed laser capture microdissection of HCC-infiltrating and noncancerous liver-infiltrating mononuclear inflammatory cells in patients with chronic hepatitis C (CH-C) and examined gene expression profiles. HCC-infiltrating mononuclear inflammatory cells had an expression profile distinct from noncancerous liver-infiltrating mononuclear inflammatory cells; they differed with regard to genes involved in biological processes, such as antigen presentation, ubiquitin-proteasomal proteolysis, and responses to hypoxia and oxidative stress. Immunohistochemical analysis and gene expression databases suggested that the up-regulated genes involved macrophages and Th1 and Th2 CD4 cells. We next examined the gene expression profile of peripheral blood mononuclear cells (PBMC) obtained from CH-C patients with or without HCC. The expression profiles of PBMCs from patients with HCC differed significantly from those of patients without HCC ($P < 0.0005$). Many of the up-regulated genes in HCC-infiltrating mononuclear inflammatory cells were also differentially expressed by PBMCs of HCC patients. Analysis of the commonly up-regulated or down-regulated genes in HCC-infiltrating mononuclear inflammatory cells and PBMCs of HCC patients showed networks of nucleophosmin, SMAD3, and proliferating cell nuclear antigen that are involved with redox status, the cell cycle, and the proteasome system, along with immunologic genes, suggesting regulation of anticancer immunity. Thus, exploring the gene expression profile of PBMCs may be a surrogate approach for the assessment of local HCC-infiltrating mononuclear inflammatory cells. [Cancer Res 2008;68(24):10267–79]

Introduction

Hepatocellular carcinoma (HCC) is one of the most frequent malignancies worldwide (1). It commonly develops from chronic liver diseases, such as viral hepatitis (2) and chronic hepatitis, resulting from hepatitis C virus (HCV) infection, is a major risk factor. Indeed, 7% of patients with liver cirrhosis (LC) caused by persistent HCV (LC-C) infection develop HCC annually (3).

Cancer tissues are often associated with infiltrating inflammatory cells, such as tumor-associated macrophages (4), T lymphocytes (5), and antigen-presenting cells (6). These tumor-infiltrating mononuclear inflammatory cells are thought to be important modulators of HCC (7). However, their actual role remains controversial. Increased numbers in HCC have been correlated with a fair prognosis (8), but tumor-infiltrating mononuclear inflammatory cells in HCC tissues have also been found to involve more $FOXP3^+$ regulatory T cells (9) and provide a cancer-favorable environment that leads to resistance to therapy. Characterization of tumor-infiltrating mononuclear inflammatory cells may be valuable in understanding tumor immunology and, possibly, in predicting the prognosis of HCC patients (7).

Peripheral blood mononuclear cells (PBMCs) consist of immune cells, such as monocytes and lymphocytes, and are essential players in the host immune defense system, which responds to various abnormal conditions in the host (10). PBMCs and tumor-infiltrating mononuclear inflammatory cells contain CTLs, specifically cytocidal to cancer tissues (11) and regulatory T cells that can suppress the host immune response against cancer (9). Thus, PBMCs may potentially reflect host immune status. However, there are limited assays for assessing the immune status of PBMCs, such as a proliferation assay, measurements of cytokine production, and the assessment of cytocidal potential.

The advent of cDNA microarray technology for the analysis of gene expression profiles has been useful in comprehensively disclosing underlying molecular features and has provided considerable information for basic science and clinical medicine. We have analyzed gene expression in liver diseases (12, 13) and believe it may become a useful diagnostic tool using liver tissue biopsy samples (14). We have also reported that gene expression profiling of PBMCs predicted the effect of IFN for the eradication of HCV (15) and can provide biomarkers not only for the control of blood sugar but also possibly for predisposing diabetic factors (16). Gene expression profiling of PBMCs from patients with renal cell carcinoma can be used to predict their response to systemic chemotherapy (17). Thus, gene expression information from the cellular components of peripheral blood may be useful in interpreting the internal condition of the patient.

In this study, we used DNA microarray technology to examine differences in gene expression profiles between HCC-infiltrating and noncancerous liver-infiltrating mononuclear inflammatory cells, which were selectively microdissected (12), and the gene expression profiles of PBMCs from LC-C patients with or without HCC. We observed distinct transcriptional features of HCC-infiltrating mononuclear inflammatory cells, reflecting the immune status of the local environment. Intriguingly, the transcriptional features of the HCC-infiltrating mononuclear inflammatory cells were shared with PBMCs from HCC patients. Thus, we suggest the possibility that the gene expression profile of PBMCs may be useful as a clinical surrogate biomarker for the assessment of

Note: Supplementary data for this article are available at Cancer Research Online (http://cancerres.aacrjournals.org/).

Requests for reprints: Shuichi Kaneko, 13-1 Takara-machi, Kanazawa, Ishikawa 920-8641, Japan. Phone: 81-76-265-2233; Fax: 81-76-234-4250; E-mail: skaneko@m-kanazawa.jp.

doi:10.1158/0008-5472.CAN-08-0911

the internal environment of HCC patients with chronic hepatitis C (CH-C) infection.

Materials and Methods

Study subjects. All patients participating in this study had advanced chronic liver disease, cirrhosis, or persistent HCV infection. Twelve patients who developed HCC as a consequence of advanced chronic liver disease related to hepatitis C and who underwent surgical treatment were enrolled (Supplementary Table S1). HCC and noncancerous liver tissues were obtained and frozen. For analysis of gene expression profiles in PBMCs, 32 LC patients without HCC and 30 LC patients with HCC (Supplementary Table S2) were included. Development of HCC was diagnosed by computed tomography (CT) or magnetic resonance imaging with contrast reagents and abdominal angiography with CT imaging in arterial and portal flow phases (18). The pathologic tumor node metastasis classification system of the Liver Cancer Study Group of Japan was used for the staging of HCC. LC was diagnosed by pathologic findings in biopsy specimens where available; otherwise, radiological imaging, platelet counts, serum hyaluronic acid levels, and indocyanine green retention rates were considered for the diagnosis of cirrhosis. The study has been approved by the institutional review board, and informed consent was obtained from all patients enrolled in the study.

Isolation of PBMCs. PBMCs were isolated from heparinized blood samples by Ficoll-Hipaque density gradient centrifugation, as reported previously (15).

Laser capture microdissection. HCC and noncancerous liver tissues obtained during surgery were frozen in optimum cutting temperature compound (Sakura Finetech; ref. 13). All HCC tissues were nodular and clearly separated by noncancerous tissues macroscopically. Cells infiltrating HCC tissues were visualized under a microscope and precisely excised by laser capture microdissection (LCM) using a CRI-337 (Cell Robotics, Inc.), as previously performed (Supplementary Fig. S1*A*; ref. 12). Cells infiltrating noncancerous tissues of CH-C patients were visualized and excised similarly.

RNA isolation and amplification. Total RNA was isolated from PBMCs or tissue samples using a microRNA isolation kit (Stratagene) in accordance with the supplied protocol with slight modifications. Isolated RNA was then amplified twice using antisense RNA and an Amino Allyl MessageAmp aRNA kit (Ambion), as described previously (13). The reference RNA sample was isolated from the PBMCs of a 29-yr-old healthy male volunteer and was amplified in the same manner. Amplified RNAs from the PBMCs of patients and the healthy volunteer were labeled with Cy5 and Cy3 (Amersham), respectively. Equal amounts of amplified RNAs were hybridized to an oligo-DNA chip (AceGene Human Oligo Chip 30K, Hitachi Software Engineering Co., Ltd.) overnight and were then washed for image scanning.

DNA microarray image analysis. The fluorescence intensity of each spot on the oligo-DNA chip was determined using a DNA Microarray Scan Array G (PerkinElmer). The images obtained were quantified using a DNASIS array (v2.6, Hitachi Software Engineering Co., Ltd). For normalization, the intensity of each spot without oligo-DNA was subtracted from that with oligo-DNA in the same block. A validated spot was determined when the intensity of the spot was within the intensity ± 2 SDs for each block. By calibrating the median to base quantity, the intensities of all spots were adjusted for normalization between Cy5 and Cy3.

Quantitative real-time detection PCR. Real-time detection PCR (RTD-PCR) was performed as previously described (15). Briefly, template cDNA was synthesized from 1 μg of total RNA using SuperScript II RT (Invitrogen). Primer pairs for chemokine (C-C motif) receptor 1 (*Ccr1*), histone acetyltransferase 1 (*Hat1*), mitogen-activated protein kinase kinase 1 interacting protein 1 (*Map2k1ip1*), phosphatidylinositol glycan anchor biosynthesis, class B (*PigB*), toll-like receptor 2 (*Tlr2*), superoxide dismutase 2 (*Sod2*), cytokeratin 8 (*Krt8*), *Krt18*, *Krt19*, and glyceraldehydes-3-phosphate dehydrogenase, as an internal control of expression, were purchased from the TaqMan assay reagents library (Applied Biosystems). Synthesized cDNA was mixed with the TaqMan Universal Master Mix (Applied Biosystems), as well as each primer pair and reaction was performed using ABI PRISM 7900HT. Relative expression level of each gene was calculated compared with that of internal control in each sample. Results are expressed as means ± SE.

Flow cytometry analysis. Flow cytometry analysis was performed as described previously (19). Briefly, isolated PBMCs were incubated in PBS supplemented with 2% bovine serum albumin (Sigma-Aldrich JAPAN K.K.) with antihuman CCR1 and CCR2 antibodies labeled with Alexa Fluor 647 (Becton Dickinson Pharmingen). The fluorescence intensity of the cells was measured using a FACSort (Becton Dickinson).

Immunohistochemistry. Surgically obtained HCC and noncancerous liver tissues were fixed with neutral buffered formalin, embedded in paraffin, cut into 4-μm sections, and mounted on microscope slides. The fixed slides were deparaffinized and subjected to heat-induced epitope retrieval 98°C for 40 min. After blocking endogenous peroxidase activity in the tissue specimen using 3% hydrogen peroxide, the slides were incubated with appropriately diluted primary antibodies, antihuman CD4 or antihuman CD14 mouse monoclonal antibodies (Visionbiosystems Novocastra). The reaction was visualized by the REAL EnVision Detection System (DAKO) followed by counterstaining with hematoxylin.

Statistical analysis. Hierarchical clustering and principal component analysis of gene expression was performed using BRB-ArrayTools.[1] Fisher's exact test was used to examine the significance of hierarchical clustering in the dendrogram. A class prediction was performed by three nearest neighbors, incorporating genes that were differentially expressed at the $P = 0.002$ significance level, as assessed by the random variance t test (BRB-ArrayTools). For genes to analyze in a pathway, we used a P value of <0.05 with 2,000 permutations to avoid underestimating the presence of meaningful signaling pathways that were coordinately up-regulated or down-regulated with subtle differences (13). The cross-validated misclassification rate was computed, and at least 2,000 permutations were performed for a valid permutation P value. The univariate t values for comparing the classes were used as weights. Student's t-test was performed for RTD-PCR data, and P values of <0.05 were deemed to be statistically significant. The population of CCR1-positive or CCR2-positive cells in PBMCs by flow cytometry analysis was tested for differences (with $P < 0.05$) by the Mann-Whitney U-test, using SPSS software (SPSS Japan, Inc.).

Analysis of expression data for biological processes and networks. As for genes significantly up-regulated or down-regulated in HCC-infiltrating mononuclear inflammatory cells compared with noncancerous liver-infiltrating mononuclear inflammatory cells or in PBMCs in LC without HCC compared with LC with HCC at $P < 0.05$, we have performed analysis of the biological processes using the MetaCore software suite (GeneGo), as described previously (13). Possible networks were created according to the list of the differentially expressed genes using the MetaCore database, a unique curated database of human protein-protein and protein-DNA interactions, transcription factors, and signaling, metabolic, and bioactive molecules. The P value was calculated as described previously (13).

Gene expression data of major leukocyte types and analysis of DNA microarray expression data. Gene expression data for leukocytes were retrieved through publicly accessible databases.[2] The gene set database GDS1775, which includes gene expression data for major leukocyte types, was obtained and subjected to one-way clustering analysis using BRB-Array Tools with genes that were up-regulated in HCC-infiltrating mononuclear inflammatory cells for the enrolled cases above.

Results

Gene expression in mononuclear inflammatory cells infiltrating into HCC tissue. HCC is frequently associated with infiltrating mononuclear inflammatory cells (20), and various attempts have been made to understand their biological significance

[1] http://linus.nci.nih.gov/BRB-ArrayTools.html
[2] http://www.ncbi.nlm.nih.gov/geo/

(8, 9, 21). We selectively obtained HCC-infiltrating mononuclear inflammatory cells by LCM and compared their gene expression profiles with those of noncancerous liver-infiltrating mononuclear inflammatory cells obtained in the same way (Supplementary Fig. S1*A*; Supplementary Table S1). The gene expression profiles of HCC-infiltrating mononuclear inflammatory cells showed that 115, 206, and 773 genes were up-regulated and 52, 114, and 750 genes were down-regulated compared with those of noncancerous liver-infiltrating mononuclear inflammatory cells at P levels of <0.005, <0.01, and <0.05, respectively (Geo accession no.[3] GSE 10461; Supplementary Fig. S1*B*).

Genes at the $P < 0.05$ level were analyzed with regard to their role in biological processes in HCC-infiltrating mononuclear inflammatory cells compared with noncancerous liver-infiltrating mononuclear inflammatory cells using the MetaCore pathway analysis software. The significant processes, in which the up-regulated genes in HCC-infiltrating mononuclear inflammatory cells were involved, included antigen presentation, an immunologically important process in antigen-presenting cells, such as monocyte/macrophages and dendritic cells (Table 1; ref. 22). The genes involved in this process were the genes for the CD1d molecule and C-type lectin domain family 4 for glycolipid antigen recognition (23, 24) and CD86, an accessory molecule indispensable for provoking an immune response (25), suggesting an activated immune reaction in these cells. The up-regulated genes in HCC-infiltrating mononuclear inflammatory cells were also involved in the ubiquitin-proteasomal proteolysis process, with significant genes, such as those encoding ubiquitin-conjugating enzymes and proteasome subunits. This process is required to eradicate unnecessary proteins, which are ubiquitinated, and then degraded in proteasomes (26). Processes related to the steps of gene expression, such as transcription by RNA polymerase II, mRNA processing, and the process of the cell cycle were also represented in the genes up-regulated in HCC-infiltrating mononuclear inflammatory cells, indicating enhanced cellular activity. Genes involved in the process of double-strand breaks, such as topoisomerase II α4 (27), and proliferating cell nuclear antigen (PCNA; ref. 28) genes involved in responses to hypoxia and oxidative stress, such as thioredoxin, peroxiredoxin, and antioxidant protein, were also up-regulated, suggesting that HCC-infiltrating mononuclear inflammatory cells were in an activated inflammatory status and under hypoxic or oxidative stress, presumably caused by the HCC. Thus, the profile of up-regulated genes in HCC-infiltrating mononuclear inflammatory cells suggested an inflammatory status, possibly triggered by antigenic stimulation of HCC tissues.

Fewer processes were identified for the down-regulated genes. One intriguing process identified was that of integrin-mediated cell matrix adhesion, suggesting that HCC-infiltrating mononuclear inflammatory cells may be less adhesive in the local tissues where they were found (Supplementary Table S3).

Subpopulation analysis of HCC-infiltrating mononuclear inflammatory cells using immunohistochemistry and transcriptional analysis. Tumor-infiltrating mononuclear inflammatory cells consist of a mixed cell population, including macrophages, effector T cells, and regulatory T cells, which have been considered to be both cancer-favorable or cancer-unfavorable (8, 21). HCC-infiltrating and noncancerous liver-infiltrating mononuclear inflammatory cells were immunohistochemically evaluated to examine the characteristics of the subpopulations. CD14-positive monocytes/macrophages were prominent in HCC-infiltrating mononuclear inflammatory cells, whereas they were rarely observed in noncancerous liver-infiltrating mononuclear inflammatory cells (Fig. 1*A*). CD4-positive helper T cells were observed in both HCC tissues and noncancerous liver tissues, although in noncancerous liver tissues, these cells tended to accumulate within the aggregates of mononuclear inflammatory cells, whereas they seemed to be scattered in HCC-infiltrating mononuclear inflammatory cells (Fig. 1*A*).

Next, we examined the genes that were significantly up-regulated in HCC-infiltrating mononuclear inflammatory cells compared with noncancerous liver-infiltrating mononuclear inflammatory cells, relative to subpopulations of leukocytes, and explored how they may be relevant to leukocyte subpopulations, using the database of the human immune cell transcriptome in the Gene Expression Omnibus[3] (Geo accession no. GDS1775), which covers 26 immune regulatory cells, such as T cells, B cells, natural killer cells, macrophages, dendritic cells, basophils, and eosinophils. Among the 206 extracted, up-regulated genes in HCC-infiltrating mononuclear inflammatory cells (at the $P < 0.01$ level), 97 annotated genes were used for one-way hierarchical clusters (Fig. 1*B*). Most genes among 97 annotated up-regulated genes in HCC-infiltrating mononuclear inflammatory cells were shown to be expressed with higher magnitude in lipopolysaccharide-stimulated or lipopolysaccharide-unstimulated macrophages than in other types of major leukocytes. The next subpopulations, including the second most number of genes for relatively high magnitude of expression, were Th1 and Th2 CD4 cells under conditions supplemented with interleukin-12 (IL-12) and IL-4, respectively (Geo accession no.[3] GSM90858), secreting Th1 and Th2 cytokine profiles, respectively, suggesting that featured genes expressed in HCC-infiltrating mononuclear inflammatory cells were indicative of CD4 helper T cells, secreting a variety of cytokines.

Thus, this expression analysis showed that, in HCC lesions with tumor antigens, there was an accumulation of antigen-presenting cells, monocyte/macrophages, and CD4 helper T cells, which were in a cytokine-secreting condition, with enhanced cellular biological activities, including ubiquitin-proteasomal proteolysis, presumably under a hypoxic and oxidative stress environment caused by the HCC. The overall inflammatory status represented by HCC-infiltrating mononuclear inflammatory cells was not determined in terms of an anticancer effect, because no obvious shift of CD4 helper T cells to the Th1 or Th2 condition was indicated.

Distinct gene expression profile of PBMCs obtained from patients with cirrhotic liver disease complicated with HCC. The HCC-infiltrating mononuclear inflammatory cells were distinct in terms of expressed genes. The putative biological processes involving these up-regulated genes in tumor-infiltrating mononuclear inflammatory cells suggested a general influence of the HCC on the local environment of the host, represented by stress-response genes. We, thus, examined whether PBMCs in the systemic circulation of the patient might also be influenced by the development of HCC. PBMCs were obtained from 30 patients with LC associated with HCC and from 32 patients with LC not associated with HCC, and the gene expression profiles were compared (Geo accession no.[3] GSE10459).

Unsupervised hierarchical clustering analysis using 17,903 filtered genes, the expression values of which were not missing in >50% of the cases, identified two major clusters of patients, with and without HCC (data not shown). To examine the reproducibility and the reliability of the clustering, we excluded

Table 1. Biological processes for genes up-regulated in HCC-infiltrating mononuclear inflammatory cells

Biological process	−log(*P*)	Gene	ID	*t* (*T/† NT)	*P*	Cellular components‡
Antigen presentation	8.526	CD163	NM_004244	3.96	0.001	M
		CD86 antigen	NM_006889	3.28	0.006	M
		IFN, α-inducible protein 6	NM_022872	2.99	0.031	M
		IFN, γ-inducible protein 30	NM_006332	2.89	0.011	M
		Fc fragment of IgG, high affinity Ia, receptor (CD64)	NM_000566	2.85	0.013	M
		C-type lectin domain family 4, member M	NM_014257	2.73	0.020	
		CD63	NM_001780	2.51	0.024	M
		CD1D antigen	NM_001766	2.19	0.049	
Ubiqutin-proteasomeal proteolysis	6.555	Nucleoporin 107 kDa	NM_020401	4.32	0.001	
		Proteasome subunit, β type, 5	NM_002797	3.80	0.002	T, M
		Ubiquitin-conjugating enzyme E2R 2	NM_017811	3.67	0.004	
		Proteasome subunit, α type, 5	NM_002790	3.64	0.003	
		Prostaglandin E synthase 3	NM_006601	3.53	0.003	
		Ubiquitin-conjugating enzyme E2 binding protein, 1	NM_005744	2.94	0.011	
		Ubiquitin-conjugating enzyme E2E 3	NM_006357	2.75	0.017	
		DnaJ (Hsp40) homologue, subfamily A, member 1	NM_001539	2.47	0.028	
		Syntaxin 5	BC012137	2.19	0.046	
ER and cytoplasm	5.704	Chaperonin containing TCP1, subunit 8 (θ)	NM_006585	3.71	0.002	T, M
		Peptidylprolyl isomerase A	NM_021130	3.69	0.002	
		ERO1-like	NM_014584	3.03	0.009	T, M
		Peptidylprolyl isomerase C	BC002678	2.68	0.017	M
		SEC63 homologue	AF119883	2.59	0.020	
		Peptidylprolyl isomerase B	NM_000942	2.54	0.023	
		Chaperonin containing TCP1, subunit 4 (δ)	NM_006430	2.53	0.023	
		FK506 binding protein 3, 25 kDa	NM_002013	2.46	0.026	T, M
		Heat shock 70 kDa protein 5	AF188611	2.45	0.027	
mRNA processing	5.143	Small nuclear ribonucleoprotein polypeptide B	NM_003092	4.65	0.000	
		Small nuclear ribonucleoprotein polypeptide F	BC002505	3.28	0.005	T
		DEAD (Asp-Glu-Ala-Asp) box polypeptide 20	NM_007204	3.22	0.006	
		Cleavage and polyadenylation specific factor 6	NM_007007	3.16	0.010	
		Cleavage stimulation factor subunit 2	NM_001325	3.10	0.008	T
		Heterogeneous nuclear ribonucleoprotein A2/B1	NM_031243	2.94	0.010	
		PRP4 pre-mRNA processing factor 4 homologue B	NM_003913	2.90	0.020	
		Gem-associated protein 4	NM_015721	2.64	0.019	T
		LSM6 homologue	NM_007080	2.63	0.019	
		Exportin 1	NM_003400	2.42	0.029	
		RNA-binding motif protein 8A	AF127761	2.41	0.030	
		Splicing factor, arginine/serine-rich 1	M72709	2.39	0.036	
Transcription by RNA polymerase II	4.298	TAF9 RNA polymerase II	NM_016283	5.01	0.001	
		General transcription factor IIH, polypeptide 3, 34 kDa	NM_001516	4.74	0.001	
		TAF6-like RNA polymerase II	NM_006473	3.91	0.002	
		Nuclear receptor corepressor 1	AF044209	3.64	0.007	
		TATA box binding protein	NM_003194	2.89	0.018	

(*Continued on the following page*)

Table 1. Biological processes for genes up-regulated in HCC-infiltrating mononuclear inflammatory cells (Cont'd)

Biological process	−log(*P*)	Gene	ID	*t* (*T/† NT)	*P*	Cellular components‡
		Cofactor required for Sp1 transcriptional activation	NM_004270	2.82	0.014	T, M
		SUB1 homologue	NM_006713	2.59	0.021	
		General transcription factor II, I	NM_033001	2.55	0.023	T, M
		GCN5-like 2	NM_021078	2.34	0.048	
		TBP-like 1	NM_004865	2.24	0.043	
Double-strand breaks repair	3.289	RAD51 homologue C	NM_058216	5.24	0.000	T
		Werner syndrome	AF091214	4.99	0.000	T
		NIMA-related kinase 1	AK027580	3.27	0.007	
		Protein phosphatase 2	AF086924	3.24	0.023	
		Protein phosphatase 6	NM_002721	3.13	0.007	
		Proliferating cell nuclear antigen	NM_002592	2.80	0.014	T
		Topoisomerase II α-4	AF285159	2.57	0.033	T
ESR1-nuclear pathway	2.886	Nuclear receptor corepressor 1	AF044209	3.64	0.007	
		Nuclear receptor coactivator 4	X77548	3.19	0.007	
		Dopachrome tautomerase	NM_001922	3.04	0.019	
		COP9, subunit 5	NM_006837	2.77	0.014	
		Tissue specific extinguisher 1	NM_002734	2.70	0.018	M
		SCAN domain containing 1	NM_033630	2.50	0.026	
		Kinase insert domain receptor	NM_002253	2.35	0.047	
Cell cycle	2.241	Cyclin-dependent kinase inhibitor 3	NM_005192	4.60	0.000	
		Erythrocyte membrane protein band 4.1	NM_004437	3.47	0.014	
		RAN, member RAS oncogene family	NM_006325	3.38	0.004	T
		Cyclin C	NM_005190	3.14	0.008	
		Cell division cycle 42	NM_044472	3.14	0.007	
		Cyclin-dependent kinase-like 1	NM_004196	2.77	0.033	
		Cell division cycle 73	NM_024529	2.72	0.043	M
		Cell division cycle 27	NM_001256	2.57	0.043	
		Microtubule-actin cross-linking factor 1	AK023285	2.57	0.025	
		Histone cluster 1	NM_005323	2.30	0.047	
		Cyclin-dependent kinase 7	NM_001799	2.13	0.050	
		Cyclin G_2	NM_004354	2.48	0.038	
Response to hypoxia and oxidative stress	1.401	Thioredoxin	NM_003329	2.64	0.019	T, M
		Glutaredoxin 2	NM_016066	2.63	0.024	T, M
		Peroxiredoxin 3	NM_006793	2.81	0.016	T, M
		Peroxiredoxin 2	NM_005809	2.27	0.039	
		Antioxidant protein 2	NM_004905	2.22	0.042	
		Peroxiredoxin 1	NM_002574	2.21	0.043	T, M
		Microsomal glutathione *S*-transferase 2	NM_002413	2.41	0.031	M

*T represents tumor-infiltrating mononuclear inflammatory cells.
†NT represents non–tumor-infiltrating mononuclear inflammatory cells.
‡Cellular components predominantly expressed cellular components among 26 immune regulatory cells (T, Th cells; M, macrophage).

unchanged genes in all samples (genes with less than a 1.8-fold difference in >85% of samples) to remove noise. This hierarchical clustering analysis using 1,917 filtered genes confirmed two clear clusters in patients with or without HCC (Fig. 2*A*). In one major cluster, including the most LC cases, there was a subcluster, LC/HCC, which included more of the HCC patients located next to the cluster of patients with HCC (LC/HCC; Fig. 2*A*). The reproducibility of the clustering (proportion, averaged over replications and over all pairs of samples in the same cluster, BRB-ArrayTools) was 93%. Sensitivity and specificity to HCC in this cluster analysis is 88% and 76%, respectively. These cirrhotic patients without HCC were followed for at least a further 12 months to detect HCC; none of those in the LC group developed HCC over this time. The principal component analysis was performed with the filtered 1,917 genes and the two major groups; classifying LC and HCC were similarly observed (Fig. 2*B*).

To further confirm that gene expression in the PBMCs of patients with HCC was distinct from that in patients without HCC, analysis of PBMC gene expression was performed by a

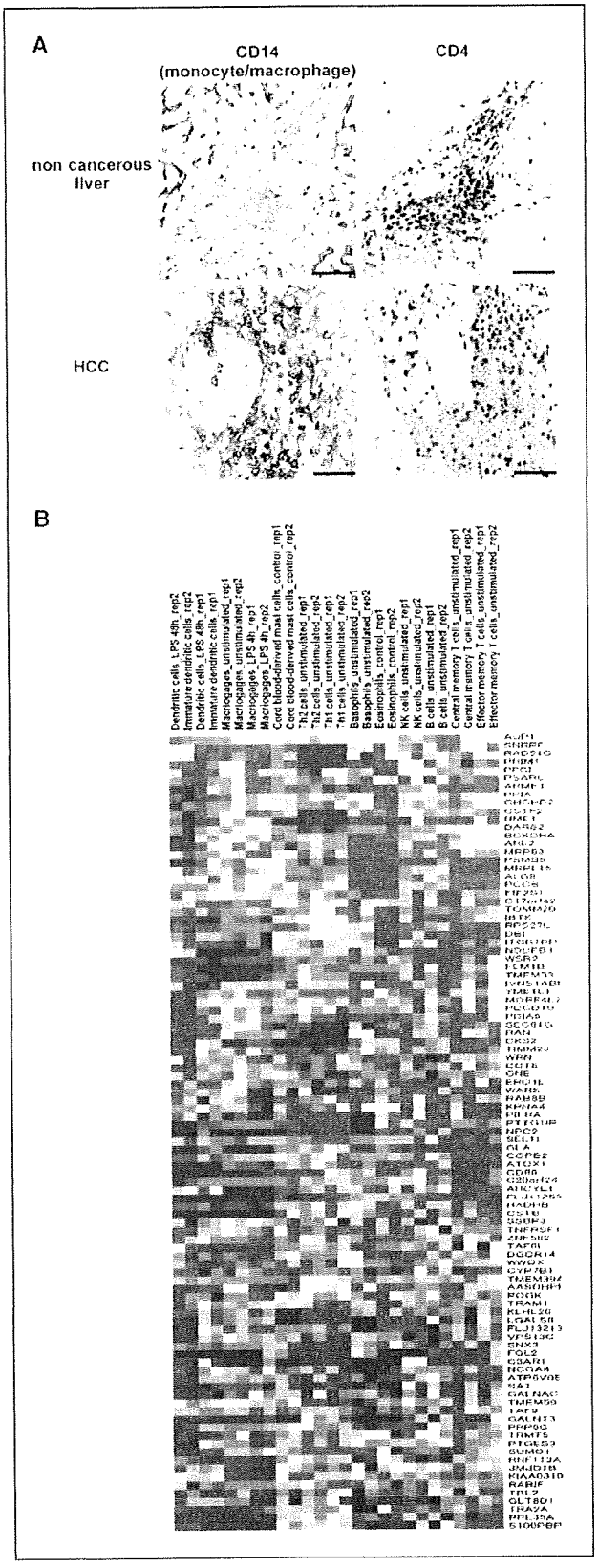

supervised learning method using categories of LC-C or HCC, age, gender, serum alanine aminotransferase (ALT), and α-fetoprotein (AFP). It showed that patients with or without HCC were significant classifiers ($P < 0.0005$), assigned with 1,430 predictor genes ($P < 0.002$; Table 2). Of 32 patients with LC, eight (25%) were misclassified as having HCC, and 2 of 30 patients with HCC (6.7%) were misclassified as not having HCC, indicating that the overall accuracy of the prediction of a patient with or without HCC was 84% (Table 2). Other clinical variables supposed to be related to HCC occurrence, such as age (ref. 29; >68 or ≤ 68 years old), gender (30), and ALT(ref. 31; >50 or ≤50 IU/L), could not differentiate gene expression in PBMCs. AFP (>20 or ≤20 ng/mL) was actually significant but was a much less powerful classifier ($P < 0.02$, assigned with 301 classifier genes). The prediction accuracy for categories of LC-C versus HCC and the AFP value >20 versus ≤20 ng/mL is not significantly affected whenever the number of predictor genes is reduced to below 62 (Supplementary Fig. S2). Taken together, these results by unsupervised and supervised analysis methods indicate that HCC development in LC-C patients significantly affects the gene expression profile in PBMCs.

Features of biological processes for which gene expression was significantly altered in PBMCs in HCC patients. We next examined the biological processes possibly affected by HCC development, given the expression profiles in PBMCs from patients with HCC. Statistical analysis showed that 867 genes were up-regulated and 989 genes were down-regulated in PBMCs from patients with HCC, compared with those without HCC ($P < 0.005$). Six representative genes, *Ccr1, Hat, Map2k1ip1, PigB, Tlr2,* and *Sod2,* were randomly selected from genes which were biologically important and differentially expressed between LC and HCC groups, and their expression was confirmed by RTD-PCR (Supplementary Fig. S3*A*). To exclude the possibility of circulating cancer cells, we have also examined the expression of *Afp, Krt8, Krt18,* and *Krt19*. No expression was detected for *Afp* (data not shown), and no statistically significant difference was found for expression of *Krt8, Krt18,* and *Krt19* between patients with HCC and without HCC (Supplementary Fig. S3*A*). The expression data were also confirmed by flow cytometric analysis. We evaluated how many cells in blood expressed CCR1 and CCR2 and confirmed that populations expressing CCR1 and CCR2 were significantly higher in PBMCs from patients with HCC than those without (Supplementary Fig. S3*B*). To understand the biological processes in PBMCs for which up-regulated or

Figure 1. HCC-infiltrating mononuclear inflammatory cells involve monocyte/macrophage and helper T cell. *A*, immunohistochemical staining. Many of the HCC-infiltrating mononuclear inflammatory cells expressed monocyte/macrophage marker, CD14. In contrast, few CD14-positive cells were seen in noncancerous liver-infiltrating mononuclear inflammatory cells. *Bars*, 100 μm. *B*, one-way hierarchical clustering analysis of gene expression of immune-mediating cells with genes whose expression was up-regulated in HCC-infiltrating mononuclear inflammatory cells. Data for gene expression in immune-mediating cells were retrieved from Gene Expression Omnibus[2] (Geo accession no. GDS 1775). By excluding genes missing from over half of the immune-mediating cells, 206 genes up-regulated in HCC-infiltrating mononuclear inflammatory cells were filtered, and the remaining 97 genes were used for clustering. Transverse and longitudinal titles show the type of immune-mediating cell and gene symbols, respectively. Color indicates relative expression magnitude of 97 up-regulated genes HCC-infiltrating mononuclear inflammatory cells among retrieved expression data of major leukocyte types deposited in the public database. The red and blue color means relatively high or low magnitude of expression among 26 retrieved expression data of leukocytes. The heat-map shows that helper T cells and unstimulated or stimulated macrophages included more blocks with the red color.

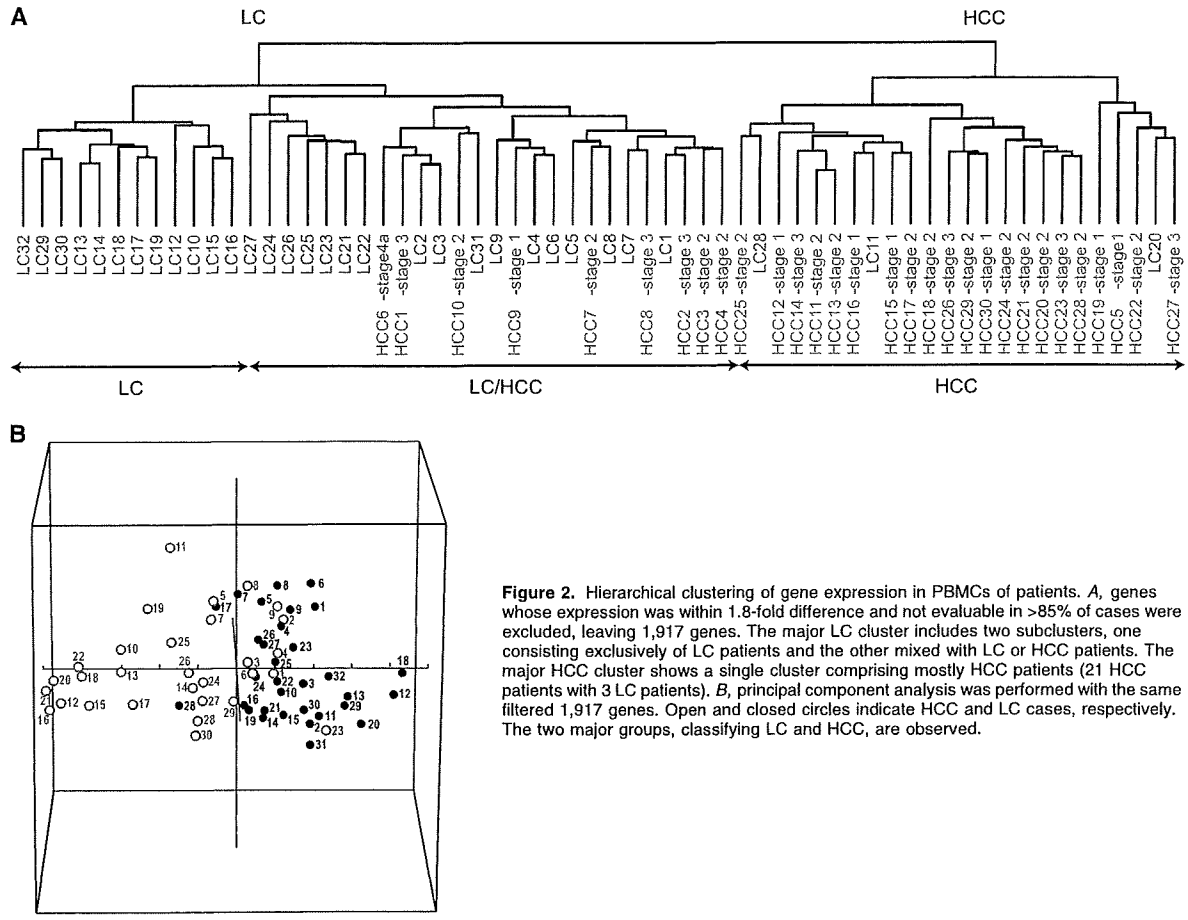

Figure 2. Hierarchical clustering of gene expression in PBMCs of patients. *A*, genes whose expression was within 1.8-fold difference and not evaluable in >85% of cases were excluded, leaving 1,917 genes. The major LC cluster includes two subclusters, one consisting exclusively of LC patients and the other mixed with LC or HCC patients. The major HCC cluster shows a single cluster comprising mostly HCC patients (21 HCC patients with 3 LC patients). *B*, principal component analysis was performed with the same filtered 1,917 genes. Open and closed circles indicate HCC and LC cases, respectively. The two major groups, classifying LC and HCC, are observed.

down-regulated genes were observed, we used MetaCore. The up-regulated genes in PBMCs from patients with HCC were involved in processes such as ubiquitin-proteasomal proteolysis (e.g., heat shock 70 kDa protein 4, ubiquitin conjugating enzymes), mRNA processing (e.g., heterogeneous nuclear ribonucleoproteins, RNA methyltransferase), antigen presentation (e.g., MHC class I polypeptide-related sequence A, B), cell cycle (e.g., HAT1, PCNA), and the response to hypoxia and oxidative stress (e.g., glutaredoxin 2, SOD2, thioredoxin; Table 3). These differentially up-regulated biological processes were also up-regulated processes in HCC-infiltrating inflammatory cells (Table 1). Thus, PBMCs from HCC patients present antigens in conditions of hypoxia and oxidative stress. Additionally, genes involved in other processes, such as apoptosis (e.g., apoptotic peptidase activating factor 1,

Table 2. Supervised learning methods for gene expression of PBMCs

Classifier category	Clinical groups	Total no. cases	No. cases misclassified	Classifier *P* values	No. genes in the classifiers ($P < 0.002$)
LC-C versus HCC	LC-C	32	8	<0.0005	1,430
	HCC	30	2		
Age (y)	>68	31	12	0.317	32
	≦68	31	16		
Gender	Male	25	15	0.178	20
	Female	37	9		
ALT (IU/L)	>50	26	20	0.82	28
	≦50	36	14		
AFP (ng/mL)	>20	29	10	0.02	301
	≦20	33	10		